Review

International Journal of Modern Physics B
Vol. 28, No. 17 (2014) 1430009 (43 pages)

DOI: 10.1142/S0217979214300096

World Scientific
www.worldscientific.com



# *Ab initio* calculations of $SrTiO_3$, $BaTiO_3$, $PbTiO_3$, $CaTiO_3$, $SrZrO_3$, $PbZrO_3$ and $BaZrO_3$ (001), (011) and (111) surfaces as well as *F* centers, polarons, KTN solid solutions and Nb impurities therein

R. I. Eglitis

*Institute of Solid State Physics,University of Latvia,*
*8 Kengaraga Str., Riga LV1063, Latvia*
*rieglitis@gmail.com*

Received 14 February 2014
Accepted 23 February 2014
Published 21 March 2014

In this paper, the review of recent results of calculations of surface relaxations, energetics, and bonding properties for $ABO_3$ perovskite (001), (011) and (111) surfaces using mostly a hybrid description of exchange and correlation is presented. Both AO and $BO_2$-terminations of the nonpolar (001) surface and A, BO, and O terminations of the polar (011) surface, as well as B and $AO_3$-terminations of the polar (111) surface were considered. On the AO-terminated (001) surface, all upper-layer A atoms relax inwards, while all second layer atoms relax outwards. For the $BO_2$-terminated (001) surface, in most cases, the largest relaxations are on the second-layer metal atoms. For almost all $ABO_3$ perovskites, the surface rumpling is much larger for the AO-terminated than for the $BO_2$-terminated (001) surface, but their surface energies are always quite similar. In contrast, different terminations of the (011) $ABO_3$ surface lead to very different surface energies for the O-terminated, A-terminated, and BO-terminated (011) surface, respectively. A considerable increase in the Ti–O or Zr–O, respectively, chemical bond covalency near the (011) surface as compared both to the bulk and to the (001) surface in $ABO_3$ perovskites were predicted. According to the results of *ab initio* calculations for Nb doped $SrTiO_3$, Nb is a shallow donor; six nearest O ions are slightly displaced outwards from the Nb ion. The *F* center in $ABO_3$ perovskites resembles electron defects in the partially-covalent $SiO_2$ crystal rather than usual *F* centers in ionic crystals like MgO and alkali halides. The results of calculations for several perovskite $KNb_xTa_{1-x}O_3$ (KTN) solid solutions, as well as hole and electron polarons in $ABO_3$ perovskites are analyzed.

*Keywords*: *Ab initio* calculations; $ABO_3$ perovskites.

PACS numbers: 68.35.Ct, 68.35.Md, 68.47.Gh

## 1. Introduction

Oxide perovskites are in demand for a variety of high-tech applications as a result of their diverse physical properties.[1–3] Thin films of $ABO_3$ perovskite ferroelectrics are

important for many industrial applications including high capacity memory cells, catalysis, optical wave guides, integrated optics applications, substrates for high-$T_c$ cuprate superconductor growth, etc.[4–6] For all these applications, the surface structure and the associated surface electronic and chemical properties are of key importance. *Ab initio* calculations of $SrTiO_3$, $BaTiO_3$, $PbTiO_3$, $CaTiO_3$, $SrZrO_3$, $PbZrO_3$ and $BaZrO_3$ surface characteristics are useful to understand processes in which surfaces play a crucial role, such as the chemistry of surface reactions, interface phenomena, and adsorption. In this study, theoretical calculations dealing with relaxed atomic structures of the $SrTiO_3$, $BaTiO_3$, $PbTiO_3$, $CaTiO_3$, $SrZrO_3$, $PbZrO_3$ and $BaZrO_3$ (001), (011) and (111) surfaces were reviewed.

Due to intensive development and progressive miniaturization of electronic devices, the surface structure as well as the electronic properties of the $ABO_3$ perovskite thin films have been extensively studied experimentally in recent years. Among all $ABO_3$ perovskites, experimentally most intensively have been studied the (001) surface of the technologically very important $SrTiO_3$ perovskite. For example, Bickel *et al.*[7] analyzed the (001) surface structure of $SrTiO_3$ at $T = 120$ K by means of low-energy-electron diffraction (LEED). They got the best theory-experiment fit results for a surface containing domains of two different layer terminations.[7] Four years later, Hikita *et al.*[8] experimentally studied the electronic and atomic structure of $TiO_2$ and SrO terminated $SrTiO_3$ (100) surface using reflection high energy electron diffraction (RHEED), X-ray photoelectron spectroscopy (XPS) and UPS. According to their results, the oxygen atoms on the outermost $SrTiO_3$ surface are pulled out for 0.10 Å and 0.16 Å, respectively.[8] Note, however, that the LEED[7] and RHEED[8] experiments contradict each other in the sign of the near-surface interplanar separation between the first and the second surface plane $\Delta d_{12}$ for SrO-terminated $SrTiO_3$ (001) surface. Ikeda *et al.*[9] determined the surface relaxation and rumpling of $TiO_2$-terminated $SrTiO_3$ (001) surface by means of medium energy ion scattering (MEIS). Charlton *et al.*[10] used the X-ray diffraction in order to determine the 300 K structure of $SrTiO_3$ (001) $1 \times 1$ with a termination of 78% TiO and 22% of SrO. Their data indicated that a lateral ferroelectric distortion was absent on both terminations.[10] Van der Heide *et al.*[11] analyzed the chemical and structural properties of several $SrTiO_3$ (001) surfaces prior to and following UHV and $O_2$ annealing using XPS, time-of-flight and recoiling spectrometry (TOF-SARS), and LEED. Their simulations of the TOF-SARS azimuthal scans indicated that the O atoms are located 0.1 Å above the Ti-terminated surface layer.[11] Maus-Friedrichs *et al.*[12] experimentally investigated the $SrTiO_3$ (001) surface with the metastable impact electron spectra (MIES) and ultraviolet photoelectron spectroscopy (UPS) methods, as well as performed complementary *ab initio* calculations.[12]

Enterkin *et al.*[13] reported a solution to the $3 \times 1$ $SrTiO_3$ (110) surface structure obtained through transmission electron diffraction, and confirmed through density functional theory (DFT) calculations and scanning tunneling microscopy (STM) images and simulations.[13] In contrast to $ABO_3$ perovskite (001) surfaces, their (011) surfaces are experimentally considerably less studied. Most of the experimen-

tal work dealing with $ABO_3$ perovskite (011) surfaces was focused on the $SrTiO_3$ (011) surface using STM, UPS, XPS techniques, Auger spectroscopies, and LEED experiments.[14–20]

There exist several experimental studies dealing with $SrTiO_3$ (111) surfaces. For example, Tanaka and Kawai have obtained clean surfaces of reduced $SrTiO_3$ (111) crystals and observed them by means of STM combined with reflection high energy diffraction. They have observed two different surface structures. One obtained by annealing at the temperature $\sim 1.180°C$, is assigned to have a $SrO_3$ outermost layer. The other, obtained by annealing at the temperature $\sim 1.220°C$, is assigned to have a Ti outermost layer.[21] More than 10 years later Chang *et al.*[22] also reproducibly obtained an atomically well-defined $SrTiO_3$ (111) surface by a combined chemical etching and thermal annealing process.

It is not surprising that the high technological importance of $SrTiO_3$, $BaTiO_3$, $PbTiO_3$, $CaTiO_3$, $SrZrO_3$, $PbZrO_3$ and $BaZrO_3$ perovskites has motivated several *ab initio* and classical shell-model studies of their (001) surfaces.[23–82] $ABO_3$ perovskite (011) surfaces, in general, and $SrTiO_3$ (011) surfaces, in particular, are considerably less well studied than the corresponding (001) surfaces. Due to the very complex polar structure, only very few *ab initio* studies of $ABO_3$ perovskite (011) surfaces exist. The first *ab initio* study of the electronic and atomic structures of several $(1 \times 1)$ terminations of the (011) polar orientation of the $SrTiO_3$ surface was performed by Bottin *et al.*[83] One year later, Heifets *et al.*[84] performed very comprehensive *ab initio* Hartree–Fock (HF) calculations for four possible terminations (TiO, Sr, and two kinds of O terminations) of the $SrTiO_3$ (011) surface. Recently, simultaneously, Eglitis[64] and Heifets *et al.*[85] performed *ab initio* density-functional calculations of the atomic structure and charge redistribution for several different terminations of the $BaZrO_3$ (011) surfaces. Regarding other $ABO_3$ perovskite (011) surfaces, Eglitis and Vanderbilt recently performed first *ab initio* calculations based on hybrid HF and DFT exchange functionals by using Becke's three-parameter method combined with the nonlocal correlation functionals of Perdew and Wang (B3PW) for the technologically important $BaTiO_3$ and $PbTiO_3$ (011) surfaces.[47] Only two *ab initio* studies exist for the $CaTiO_3$ (011) surfaces. The *ab initio* study of $CaTiO_3$ (011) polar surfaces was performed by Zhang *et al.*[59] and recently also by Eglitis and Vanderbilt.[57] Finally, first *ab initio* calculations for $SrZrO_3$ and $PbZrO_3$ (011) surfaces were performed by Eglitis and Rohlfing.[68]

$ABO_3$ perovskite polar (111) surfaces, on the theory side, are even less studied than their (011) surfaces. Pojani *et al.*,[86] relying on the results obtained by a total energy, semi-empirical HF method, discussed polarity effects at the (111) and (110) surfaces of $SrTiO_3$. For these orientations, they considered some prototypical $(1 \times 1)$ configurations, which differ by their surface composition and the coordination number of the surface atoms. They argued that the compensation for these polar orientations is achieved through anomalous filling of surface states, which, in principle, should be detectable by surface spectroscopies. Only three theoretical

*ab initio* studies up to now exist dealing with $CaTiO_3$ (111) polar surfaces. Liu *et al.*[87] constructed the stoichiometric and nonstoichiometric terminations for the $CaTiO_3$ (111) surface. The cleavage and surface energies, surface grand potential, and surface electronic structure have been calculated for the two main classes of terminations using an *ab initio* plane wave ultrasoft pseudopotential method based on the local density approximation (LDA). Some preliminary results of *ab initio* B3LYP calculations for $CaTiO_3$ (111) surfaces are reported in Ref. 88. One year later, Eglitis and Rohlfing[89,90] performed *ab initio* calculations dealing with $CaTiO_3$ and $SrTiO_3$ polar (111) surface relaxations, rumplings, energetics, optical bandgaps, and charge distributions using the *ab initio* code CRYSTAL and a hybrid description of exchange and correlation. Finally, Eglitis performed the first *ab initio* calculations for polar $BaTiO_3$, $BaZrO_3$ and $SrZrO_3$ (111) surfaces.[91–93]

$ABO_3$ perovskite-type oxide crystals have numerous technological applications, and in particular, $KNbO_3$, $KTaO_3$ and their solid solutions $KTa_{1-x}Nb_xO_3$ (KTN) are used in electro-optics, holography, and second-harmonic generation applications.[94] As the temperature decreases, $KNbO_3$ goes through three ferroelectric phase transitions, whereas $KTaO_3$ is only an *incipient* ferroelectric which becomes ferroelectric already at very low Nb impurity concentrations, $x \geq 0.01$. This raises a question about the nature of the phase transition in KTN.[95] XPS has shown[96] that Ta ions are replaced by the Nb ions. Additionally XAFS measurements[95] have demonstrated that the Nb sits in off-center positions. Its [111] displacement is 0.145 Å at 70 K, and changes less than 20% as the temperature increases to the room temperature.

Nb-doped $SrTiO_3$ is also important for several high tech applications including anodes and cathodes of solid oxide fuel cells[97,98] and nonvolatile resistive switching memories.[99] Donor-doped $SrTiO_3$ ceramics have found applications also in sensors, varistors, grain boundary layer capacitors and catalysts. For these reasons, a detailed understanding of the bulk and surface structure and electronic properties of Nb doped $SrTiO_3$ is of primary importance. Considering high technological importance of Nb doped $SrTiO_3$, it is not surprising that during the last years it has been the subject of many experimental studies,[100–102] but better theoretical understanding is still necessary. The existing *ab initio* calculations were performed using DFT method combined with the plane wave basis set (BS) (CASTEP computer code),[103] full-potential linearized augmented plane waves (FLAPW)[104] and linear muffin–tin orbital approach (LMTO-ASA).[105] The common disadvantage of the DFT method is considerable underestimate of the bandgap of solids, typically 1.5–2.0 eV for $SrTiO_3$ instead of the experimental value of 3.3 eV. Due to this fact in most DFT calculations, energy levels of donors fall erroneously into the conduction band. The second DFT problem is lack of analysis of effective atomic charges and charge redistribution caused by defects. Lastly, in most of these calculations rather small supercells were used, which do not eliminate artificial interaction of periodically distributed Nb ions. Finally, Eglitis and Kotomin[106] performed the HF calculations, which typically overestimates the bandgap.

Along with the impurities, most of the real crystals are nonstoichiometric and thus contain large concentration of intrinsic defects vacancies. Oxygen vacancies are known to give rise to $F^+$ and $F$ centers (vacancy with trapped one or two electrons, respectively).[107–110] Properties of $F$-type centers, as well as hole and electron polarons, in ionic oxides are well studied. In this paper, the latest results dealing with large-scale computer modeling of basic point defects — $F$ centers, hole and electron polarons in $ABO_3$ perovskites were discussed.



## 2. Preliminaries

### 2.1. *Computational method for surface calculations*

First-principles calculations in the framework of DFT using the CRYSTAL computer code[111] have been carried out. Unlike the plane-wave codes employed in many previous studies,[112,113] CRYSTAL uses localized Gaussian-type BSs. In calculations by Eglitis and co-workers, the BSs were developed for $SrTiO_3$, $BaTiO_3$ and $PbTiO_3$ in Ref. 114. In this paper, for most of the calculations, for O atoms, this new BS which differs from previous calculations[29,30] by inclusion of polarizable $d$-orbitals on O ions were used. The CRYSTAL BS are believed to be largely transferable, so that, once determined for some chemical constituent, they may be successfully applied in the calculations for a variety of chemical substances, for example $SrF_2$, $BaF_2$ and $CaF_2$,[115–124] where the latter participates. Most of the calculations in this review were performed using the hybrid exchange-correlation B3PW functional involving a mixture of nonlocal Fock exact exchange, local-density approximation (LDA) exchange, and Becke's gradient corrected exchange functional,[125] combined with the nonlocal gradient corrected correlation potential of Perdew and Wang.[126–128] The hybrid B3PW functional for most of $ABO_3$ perovskite surface studies were selected because it yields excellent results for the $SrTiO_3$, $BaTiO_3$, and $PbTiO_3$ bulk lattice constant and bulk modulus.[29,114]

The reciprocal-space integration was performed by sampling the Brillouin zone, in most cases, with an $8 \times 8 \times 8$ Pack–Monkhorst mesh,[129] which provides a balanced summation in direct and reciprocal spaces. To achieve high accuracy, large enough tolerances of 7, 8, 7, 7 and 14 were chosen for the dimensionless Coulomb overlap, Coulomb penetration, exchange overlap, first exchange pseudo-overlap, and second exchange pseudo-overlap parameters, respectively.[111] An advantage of the CRYSTAL code is that it treats isolated two-dimensional slabs, without any artificial periodicity in the $z$ direction perpendicular to the surface, as commonly employed in most previous surface band-structure calculations (e.g., Ref. 41).

The elastic constants are calculated in the standard way.[111,130] The bulk modulus could be calculated in two ways, first as

$$B = \frac{2}{9V_0}\frac{\partial^2 E_{\text{un.cell}}}{\partial V^2}, \tag{1}$$

or using the elastic constants[111]:

$$B = (C_{11} + 2C_{12})/3\,. \tag{2}$$

The results for both type of bulk modulus were presented in Ref. 114.

### 2.2. *$ABO_3$ perovskite surface geometries*

The $SrTiO_3$ (001) surfaces were modeled using symmetric (with respect to the mirror plane) slabs consisting of seven alternating $TiO_2$ and SrO layers, respectively. (Henceforth, $SrTiO_3$ will be used for presentation purposes, but everything that is said will apply equally to the $BaTiO_3$, $PbTiO_3$, $CaTiO_3$, $SrZrO_3$, $PbZrO_3$ and $BaZrO_3$ cases). One of these slabs was terminated by SrO planes for the $SrTiO_3$ crystal and consisted of a supercell containing 17 atoms. The second slab was terminated by $TiO_2$ planes and consisted of a supercell containing 18 atoms. These slabs are nonstoichiometric, with unit cell formulas $Sr_4Ti_3O_{10}$ and $Sr_3Ti_4O_{11}$ for the $SrTiO_3$ perovskite. These two (SrO and $TiO_2$) terminations are the only two possible flat and dense (001) surfaces for the $SrTiO_3$ perovskite lattice structure. The sequence of layers with definition of surface rumpling $s$ and the near-surface interplanar separations $\Delta d_{12}$ and $\Delta d_{23}$ at the $TiO_2$-terminated (001) surface of $SrTiO_3$ is illustrated in Fig. 1.

Unlike the (001) cleavage of $SrTiO_3$, which naturally gives rise to nonpolar SrO and $TiO_2$ terminations, a naive cleavage of $SrTiO_3$ to create (011) surfaces leads to the formation of polar surfaces. For example, the stacking of the $SrTiO_3$ crystal along the [011] direction consists of alternating planes of $O_2$ and SrTiO units having nominal charges of $-4e$ and $+4e$, respectively, assuming $O^{2-}$, $Ti^{4+}$, and $Sr^{2+}$ constituents. Thus, a simple cleavage leads to $O_2$-terminated and SrTiO-terminated (011) surfaces that are *polar* and have nominal surface charges of $-2e$ and $+2e$

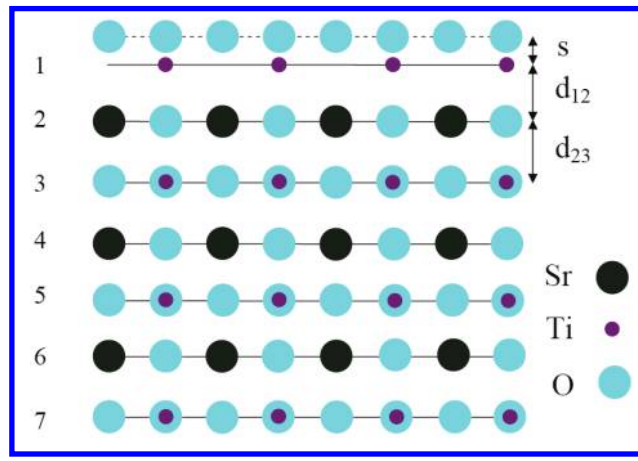


Fig. 1. $TiO_2$-terminated $SrTiO_3$ (001) surface with definitions of surface rumpling $s$ and the near-surface interplanar separations $\Delta d_{12}$ and $\Delta d_{23}$.

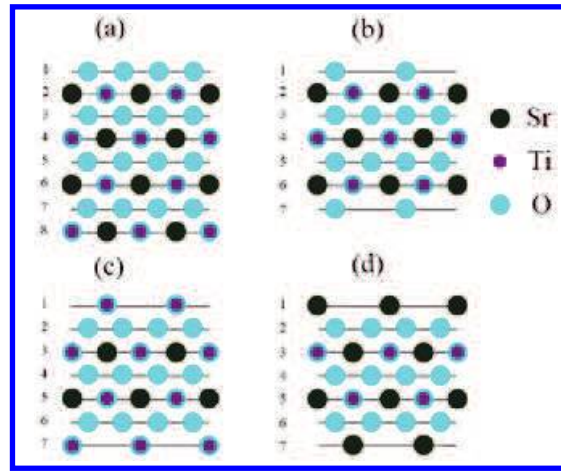


Fig. 2. Side views of slab geometries used to study $SrTiO_3$ (011) surfaces. (a) Stoichiometric eight-layer slab with $O_2$-terminated and SrTiO-terminated surfaces at top and bottom, respectively. (b) Seven-layer slab with O-terminated surfaces. (c) Seven-layer slab with TiO-terminated surfaces. (d) Seven-layer slab with Sr-terminated surfaces.

per surface cell, respectively. These are shown as the top and bottom surfaces in Fig. 2(a), respectively. If uncompensated, the surface charge would lead to an infinite electrostatic cleavage energy. In reality, the polar surfaces would probably become metallic in order to remain neutral, but in view of the large electronic gaps in the perovskites, such metallic surfaces would presumably be unfavorable. Thus, we may expect rather generally that such polar crystal terminations are relatively unstable in this class of materials.[4]

On the other hand, if the cleavage occurs in such a way as to leave a half layer of $O_2$ units on each surface, we obtain the nonpolar surface structure shown in Fig. 2(b). Every other surface O atom has been removed, and the remaining O atoms occupy the same sites as in the bulk structure. We shall refer to this as the "O-terminated" (011) surface, in distinction to the "$O_2$-terminated" polar surface already discussed in Fig. 2(a). The nonpolar nature of the O-terminated surface can be confirmed by nothing that the 7-layer 15-atom $Sr_3Ti_3O_9$ slab shown in Fig. 2(b), which has two O-terminated surfaces, is neutral. It is also possible to make nonpolar TiO-terminated and Sr-terminated surfaces, as shown in Figs. 2(c) and 2(d), respectively. This is accomplished by splitting a SrTiO layer during cleavage, instead of splitting an $O_2$ layer. For the TiO- and Sr-terminated surfaces, we use seven-layer slabs having composition $Sr_2Ti_4O_{10}$ (16 atoms) and $Sr_4Ti_2O_8$ (14 atoms) as shown in Figs. 2(c) and 2(d), respectively. These are again neutral, showing that the surfaces are nonpolar (even though they no longer have precisely the bulk $SrTiO_3$ stoichiometry).

As a next step, the $ABO_3$ perovskite (111) surfaces will be discussed. For example, in Ref. 92, the $BaZrO_3$ (111) surfaces have been modeled with two-dimensional

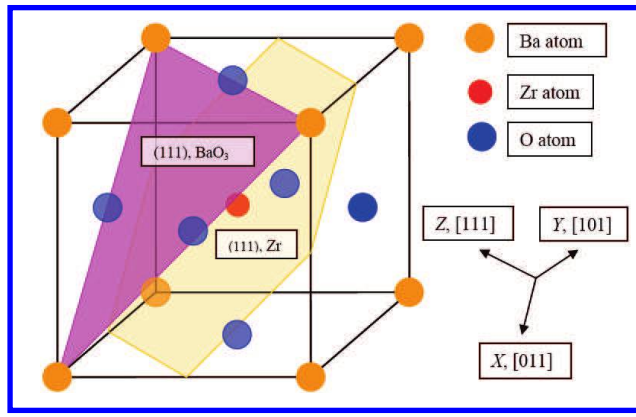


Fig. 3. Sketch of the cubic $BaZrO_3$ perovskite structure showing two possible (111) surface terminations: $BaO_3$ and Zr.

(2D) slabs, consisting of nine planes perpendicular to the [111] crystal direction. To simulate $BaZrO_3$ (111) surfaces, symmetrical slabs consisting of nine alternating Zr and $BaO_3$ layers were used (see Fig. 3). One of these slabs is terminated by Zr planes and consists of a supercell containing 21 atoms (Zr–$BaO_3$–Zr–$BaO_3$–Zr–$BaO_3$–Zr–$BaO_3$–Zr) [see Fig. 4(a)]. The second slab is terminated by $BaO_3$ planes and consists of a supercell containing 24 atoms ($BaO_3$–Zr–$BaO_3$–Zr–$BaO_3$–Zr–$BaO_3$–Zr–$BaO_3$) [see Fig. 4(b)]. These slabs are nonstoichiometric, with unit cell formulas $Ba_4Zr_5O_{12}$ and $Ba_5Zr_4O_{15}$, respectively (see Fig. 3). As it is well known from previous studies dealing with polar $CaTiO_3$ and $SrTiO_3$ (111) surfaces,[86–89,131] a strong electron redistribution takes place for such terminations in order to cancel the polarity, but the Zr or $BaO_3$-terminated $BaZrO_3$ (111) surface keeps its insulating character, and

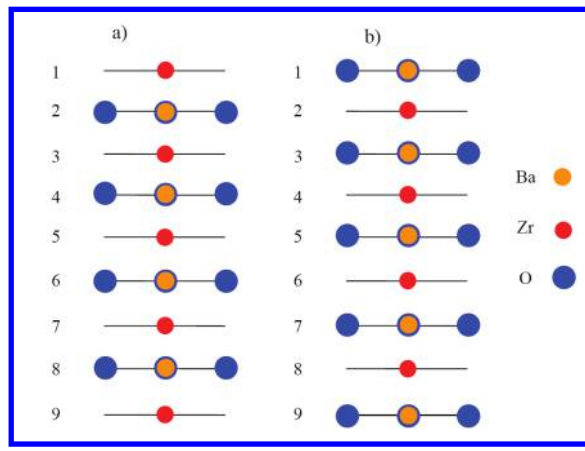


Fig. 4. Sketch of the side views of slab geometries used to study $BaZrO_3$ (111) surfaces. (a) Non-stoichiometric nine-layer slab with Zr-terminated surfaces. (b) Nonstoichiometric nine-layer slab with $BaO_3$-terminated surfaces.

such calculations are feasible. Of course, it is not possible to perform calculations for asymmetric slabs with different terminations, for example, Zr–$BaO_3$–Zr–$BaO_3$–Zr–$BaO_3$–Zr–$BaO_3$, since this would lead to a large dipole moment for an asymmetric slab.

The second well established approach for $ABO_3$ perovskite polar (111) surface calculations, which was not used by Eglitis *et al.*[87] for $SrTiO_3$, $BaTiO_3$, $CaTiO_3$, $SrZrO_3$ and $BaZrO_3$ (111) surfaces, is artificial modification of surface structure by removing O atoms from the $BaO_3$-terminated $BaZrO_3$ (111) surface and adding O atoms onto the Zr-terminated surface, respectively. Such surface structure changes, ($BaO_2$–Zr–$BaO_3$–Zr–$BaO_3$–Zr–$BaO_3$–Zr–$BaO_2$) or (ZrO–$BaO_3$–Zr–$BaO_3$–Zr–$BaO_3$–Zr–$BaO_3$–ZrO) can, in principle, provide the polarity compensation and calculations for such artificially neutral $BaZrO_3$ (111) surfaces may also be feasible.

### 2.3. *$ABO_3$ perovskite surface energies*

In order to calculate $ABO_3$ perovskite, for example, the $SrZrO_3$ (001) surface energy, I started with the cleavage energy for unrelaxed SrO- and $ZrO_2$-terminated (001) surfaces. Surfaces with both terminations simultaneously arise under (001) cleavage of the crystal, and I adopt the convention that the cleavage energy is equally distributed between the created surfaces. In my calculations, the nine-layer SrO-terminated (001) slab with 22 atoms and the $ZrO_2$-terminated one with 23 atoms represent, together, nine bulk unit cells (45 atoms) so that

$$E^{\rm unr}_{\rm surf}(\Omega) = \frac{1}{4}[E^{\rm unr}_{\rm slab}({\rm SrO}) + E^{\rm unr}_{\rm slab}({\rm ZrO_2}) - 9E_{\rm bulk}]\,, \tag{3}$$

where $\Omega$ denotes SrO or $ZrO_2$, $E^{\rm unr}_{\rm slab}(\Omega)$ are the unrelaxed energies of the SrO- or $ZrO_2$-terminated (001) slabs, $E_{\rm bulk}$ is the energy per bulk unit cell, and the factor of 1/4 comes from the fact that I create four surfaces upon the crystal cleavage procedure. Next, I can calculate the relaxation energies for each of SrO and $ZrO_2$ terminations, when both sides of the slabs relax, according to

$$E_{\rm rel}(\Omega) = \frac{1}{2}[E^{\rm rel}_{\rm slab}(\Omega) - E^{\rm unr}_{\rm slab}(\Omega)]\,, \tag{4}$$

where $E^{\rm rel}_{\rm slab}(\Omega)$ is the slab energy after relaxation (and again $\Omega$ = SrO or $ZrO_2$). The surface energy is then defined as a sum of the cleavage and relaxation energies,

$$E_{\rm surf}(\Omega) = E^{\rm unr}_{\rm surf}(\Omega) + E_{\rm rel}(\Omega)\,. \tag{5}$$

In order to calculate the $SrZrO_3$ (011) surface energies for the ZrO- and Sr-terminated surfaces, I consider the cleavage of eight bulk unit cells (40 atoms) to result in the ZrO- and Sr-terminated slabs, containing 21 and 19 atoms, respectively. I again divide the cleavage energy equally between these two surfaces and obtain

$$E^{\rm unr}_{\rm surf}(\Omega) = \frac{1}{4}[E^{\rm unr}_{\rm slab}({\rm Sr}) + E^{\rm unr}_{\rm slab}({\rm ZrO}) - 8E_{\rm bulk}]\,, \tag{6}$$

where Ω denotes Sr or ZrO, $E_{\rm slab}^{\rm unr}(\Omega)$ is the energy of the unrelaxed Sr- or ZrO-terminated (011) slab, and $E_{\rm bulk}$ is the $SrZrO_3$ energy per bulk unit cell.

Finally, when I cleave the $SrZrO_3$ crystal in another way, I obtain two identical O-terminated (011) surface slabs containing 20 atoms each. This allows for me to simplify the calculations since the unit cell of the nine-plane O-terminated (011) slab contains four bulk unit cells. Therefore, the relevant surface energy is

$$E_{\rm surf}({\rm O}) = \frac{1}{2}[E_{\rm slab}^{\rm rel}({\rm O}) - 4E_{\rm bulk}]\,, \tag{7}$$

where $E_{\rm surf}({\rm O})$ and $E_{\rm slab}^{\rm rel}({\rm O})$ are the surface energy and the relaxed slab total energy for the O-terminated (011) surface. The $ABO_3$ perovskite polar (111) surface energy calculations, using as an example the $BaZrO_3$ crystal, were discussed in Ref. 92.

### 2.4. *Intermediate neglect of different overlap (INDO) method*

For defect calculations in $ABO_3$ perovskites the INDO method was used. The calculation scheme of the Hartree–Fock–Roothaan method in the INDO approximation is discussed in detail in Refs. 132–134. Basically, the procedure reduces to diagonalizing the matrix of the Fock operator to get the one-electron energies, and the linear combination of matrix elements with appropriate weights, depending on the occupation of corresponding one-electron states, provides the total energy. The fixed BS, for example for $KNbO_3$, is minimal in the sense that each of the atom-centered functions related to the valence-band states (four in total per oxygen atom, nine per transition-metal atom) is encountered only once. The construction of the on-site and off-diagonal parts of the Fock matrix is determined in terms of several empirical parameters, labeled by the atom type $A$ and the index of the atomic orbital (AO) $\mu$ (see Refs. 132–134). The interaction of an electron in the $\mu$th valence AO on atom $A$ with its own core

$$U_{\mu\mu}^{A} = -E_{\rm neg}^{A}(\mu) - \sum_{\nu\in A}\left(P_{\nu\nu}^{(0)A}\gamma_{\mu\nu} - \frac{1}{2}P_{\nu\nu}^{(0)A}K_{\mu\nu}\right) \tag{8}$$

contains, apart from the $\zeta_\mu$ value, which specifies the Slater exponent for a one-exponential basis function and hence Coulomb and exchange integrals $\gamma_{\mu\nu}$ and $K_{\mu\nu}$, the initial guesses for the diagonal elements of the density matrix $P_{\mu\mu}^{(0)A}$ and for the energy of $\mu$th AO $E_{\rm neg}^{A}(\mu)$, i.e., the ion's electronegativity. The interaction of the $\mu$th AO with the core of another atom $B$ is approximated as

$$V_{\mu}^{B} = Z_B[1/R_{AB} + [\langle\mu\mu|\nu\nu\rangle - 1/R_{AB}]\exp(-\alpha_{AB}R_{AB})]\,, \tag{9}$$

where $R_{AB}$ is the distance between atoms $A$ and $B$, $Z_B$ is the core charge of atom $B$, and parameter $\alpha_{AB}$ describes the nonpoint character of this interaction.

Finally, the resonance-integral parameter $\beta_{\mu\nu}$ enters the off-diagonal Fock matrix elements for the spin component $u$

$$F_{\mu\nu}^{u} = \beta_{\mu\nu}S_{\mu\nu} - P_{\mu\nu}^{u}\langle\mu\mu|\nu\nu\rangle\,, \tag{10}$$

where the $\mu$th and $\nu$th AO are centered at different atoms, $S_{\mu\nu}$ is the overlap matrix between them, and $\langle\mu\mu|\nu\nu\rangle$ are two-electron integrals. Parameters $\zeta_\mu$, $\beta_{\mu\nu}$, $\alpha_{AB}$ and $E^A_{\text{neg}}(\mu)$ are usually fixed throughout the iterations, whereas $P^{(0)A}_{\nu\nu}$ may be corrected as the self-consistency is being achieved.

## 3. Main Results

### 3.1. *$ABO_3$ perovskite (001) surface structure*

In order to check how sensitive $ABO_3$ perovskite surface relaxation properties are to details of the *ab initio* methods used in calculations, i.e., exchange–correlation functionals, pseudopotentials, and localized/plane wave BS, in Refs. 29 and 114 were performed a detailed comparative study based on a number of different techniques. Several methods were employed: HF with different DFT-type *a posteriori* electron correlation corrections to the total energy[135] such as generalized gradient approximation (HFGGA), Perdew-91 (HFPer91), Lee, Yang, Parr (HFLYP) and full-scale DFT calculations based on the Kohn–Sham equation with a number of exchange–correlation functionals, including LDA, generalized gradient approximations (GGA) by Perdew and Wang (PW), Perdew, Burke, and Ernzerhof (PBE), as well as Becke exchange functional with Lee–Yang–Parr correlation functional (BLYP). Also a comparison with hybrid HF–DFT exchange functionals were included, in which HF exchange was mixed with DFT exchange functionals using Becke's three parameter method, combined with the nonlocal correlation functionals by Perdew and Wang (B3PW), as those by Lee, Yang, and Parr (B3LYP). For all calculations, the CRYSTAL computer code was used (see Ref. 111, and references therein for all mentioned techniques), in which both (HF/DFT) types of calculations are implemented on equal grounds.

Before starting the $ABO_3$ perovskite (001), (011) and (111) surface structure calculations, these methods were tested on the bulk properties, the lattice constant $a_0$, the bulk modulus $B$ and the elastic constants $C$ (see Table 1). It is clear from Table 1 that the LDA calculations, as usually, underestimate the lattice constant for six from seven calculated $ABO_3$ perovskites. The only exception is $SrZrO_3$, where the LDA slightly overestimate the lattice constant. The LDA is known to generally underestimate lattice parameters of solids, typically by 1%–3%. This is a serious problem for the study of ferroelectric perovskites using the LDA. As we can see from Table 1, in most cases, pure HF and GGA overestimate the $ABO_3$ perovskite lattice constant. The different GGA schemes give quite good results only for $PbTiO_3$ crystal. The $PbTiO_3$ lattice constants computed using PWGGA and PBE functionals are close to the experimental values, whereas in other cases the DFT–GGA gives mostly overestimated values. The best agreement with experimental lattice constant, on the average, was obtained for the hybrid DFT B3PW method.

Table 1 also lists the computed bulk modulus and the static elastic constants obtained by means of all methods. The presented results for both ways of bulk

Table 1. The optimized lattice constant $a_0$ (Å), bulk modulus $B$ (GPa) and elastic constants $C_{ij}$ (in $10^{11}$ dyne/cm$^2$) for seven $ABO_3$ perovskites as calculated using DFT and HF methods.

| Crystal | Property | LDA | PWGGA | PBE | BLYP | B3PW | B3LYP | HF | Exp |
|---|---|---|---|---|---|---|---|---|---|
| $SrTiO_3$ | $a_0$ | 3.86[a] | 3.95[a] | 3.94[a] | 3.98[a] | 3.90[a] | 3.94[a] | 3.92[a] | 3.89[b] |
| | $C_{11}$ | 42.10[a] | 31.29[a] | 31.93[a] | 29.07[a] | 31.60[a] | 32.83[a] | 41.68[a] | 31.72[c] |
| | $C_{12}$ | 12.21[a] | 9.80[a] | 9.75[a] | 9.39[a] | 9.27[a] | 10.57[a] | 7.11[a] | 10.25[c] |
| | $C_{44}$ | 13.32[a] | 11.34[a] | 11.30[a] | 11.09[a] | 12.01[a] | 12.46[a] | 10.50[a] | 12.35[c] |
| | $B$ | 222[a] | 170[a] | 171[a] | 159[a] | 167[a] | 180[a] | 186[a] | 174[c] |
| | $B$ | 214[a] | 167[a] | 169[a] | 164[a] | 177[a] | 177[a] | 219[a] | 179[b] |
| $BaTiO_3$ | $a_0$ | 3.96[a] | 4.03[a] | 4.03[a] | 4.08[a] | 4.01[a] | 4.04[a] | 4.01[a] | 4.00[b] |
| | $C_{11}$ | 35.81[a] | 30.11[a] | 31.04[a] | 28.22[a] | 31.12[a] | 29.75[a] | 30.07[a] | 20.60[b] |
| | $C_{12}$ | 11.52[a] | 10.35[a] | 10.72[a] | 10.78[a] | 11.87[a] | 11.57[a] | 13.46[a] | 14.00[b] |
| | $C_{44}$ | 14.98[a] | 13.22[a] | 13.98[a] | 12.24[a] | 14.85[a] | 14.54[a] | 17.34[a] | 12.60[b] |
| | $B$ | 196[a] | 169[a] | 175[a] | 166[a] | 183[a] | 176[a] | 190[a] | 162[b] |
| | $B$ | 204[a] | 175[a] | 180[a] | 154[a] | 188[a] | 172[a] | 194[a] | 195 ± 5[d] |
| $PbTiO_3$ | $a_0$ | 3.93[a] | 3.96[a] | 3.96[a] | 4.02[a] | 3.93[a] | 3.96[a] | 3.94[a] | 3.97[e] |
| | $C_{11}$ | 45.03[a] | 32.47[a] | 4.25[q] | 23.03[a] | 43.04[a] | 34.42[a] | 39.83[a] | 22.90[f] |
| | $C_{12}$ | 26.14[a] | 15.81[a] | 15.52[a] | 9.93[a] | 24.95[a] | 18.08[a] | 16.90[a] | 10.10[f] |
| | $C_{44}$ | 11.28[a] | 10.69[a] | 10.96[a] | 8.25[a] | 10.93[a] | 10.35[a] | 17.20[a] | 10.00[f] |
| | $B$ | 324[a] | 213[a] | 217[a] | 143[a] | 310[a] | 235[a] | 16.90[a] | 144[f] |
| | $B$ | 321[a] | 246[a] | 252[a] | 140[a] | 279[a] | 242[a] | 299[a] | |
| $CaTiO_3$ | $a_0$ | 3.825[j] | | 3.87[i] | | 3.85[g] | 3.85[k] | 3.90[h] | |
| $BaZrO_3$ | $a_0$ | 4.16[p] | 4.25[q] | 4.24[o] | | 4.23[l] | 4.23[n] | 4.19[m] | |
| $PbZrO_3$ | $a_0$ | 4.12[u] | | | | 4.18[r] | 4.22[t] | 4.16[s] | |
| $SrZrO_3$ | $a_0$ | 4.16[y] | | 4.19[w] | | 4.17[x] | 4.20[t] | 4.11[v] | |

[a]Reference 114. [b]Reference 136. [c]Reference 137. [d]Reference 138. [e]Reference 139.
[f]Reference 140. [g]Reference 57. [h]Reference 141. [i]Reference 59. [j]Reference 142.
[k]Reference 88. [l]Reference 64. [m]Reference 143. [n]Reference 92. [o]Reference 85.
[p]Reference 144. [q]Reference 145. [r]Reference 146. [s]Reference 147. [t]Reference 68.
[u]Reference 148. [v]Reference 149. [w]Reference 150. [x]Reference 67. [y]Reference 151.

modulus evaluation differ usually no more than 10–15%. Calculations[114] confirm the tendency, well known in the literature, that the HF calculations overestimate the elastic constants. The overestimated elastic constants have also been obtained for $SrTiO_3$, $BaTiO_3$ and $PbTiO_3$ perovskites, when the DFT–LDA scheme was used. In the case of cubic $SrTiO_3$, which is experimentally well investigated, almost perfect coincidence with the experimental data for both the bulk modulus and elastic constants were obtained using B3PW and B3LYP hybrid schemes. The disagreement of elastic constants is less than 5%, and the bulk modulus practically coincide with the experimental magnitudes.

To characterize the chemical bonding and covalency effects, a standard Mulliken population analysis for the effective static atomic charges $Q$ and other local properties of the electronic structure as described in Refs. 152 and 153 were used. The results from Refs. 25, 47, 57, 64 and 68 for $SrTiO_3$, $BaTiO_3$, $PbTiO_3$, $CaTiO_3$, $BaZrO_3$, $SrZrO_3$ and $PbZrO_3$ perovskites are presented in Table 2. For example, calculated effective charges for bulk $PbTiO_3$ are $+1.354e$ for the Pb atom, $+2.341e$ for the Ti atom, and $-1.232e$ for the O atom.[47] The bond population describing the chemical bonding between Ti and O atoms is $+98me$, typical also for another $ABO_3$ perovskites. Calculated effective charges for $BaTiO_3$ bulk are +1.797e for the Ba atom, $+2.367e$ for the Ti atom, and $-1.388e$ for the O atom,[47] indicating a

Table 2. Effective charges $Q$ and bond populations $P$ of atoms in $SrTiO_3$, $BaTiO_3$, $PbTiO_3$, $CaTiO_3$, $BaZrO_3$, $SrZrO_3$ and $PbZrO_3$ bulk calculated by means of the hybrid B3PW or B3LYP method.

| | $SrTiO_3$ | | $BaTiO_3$ | | $PbTiO_3$ | | $CaTiO_3$ | | $BaZrO_3$ | | $SrZrO_3$ | | $PbZrO_3$ | |
|---|---|---|---|---|---|---|---|---|---|---|---|---|---|---|
| Prop. | Ion | B3PW | Ion | B3PW | Ion | B3PW | Ion | B3PW | Ion | B3PW | Ion | B3LYP | Ion | B3LYP |
| $Q$ | Sr | 1.871[a] | Ba | 1.797[b] | Pb | 1.354[b] | Ca | 1.782[c] | Ba | 1.815[d] | Sr | 1.880[e] | Pb | 1.368[e] |
| $P$ | | −10 | | | | 16 | | 6 | | −12 | | 2 | | 30 |
| $Q$ | O | −1.407 | O | −1.388 | O | −1.232 | O | −1.371 | O | −1.316 | O | −1.351 | O | −1.160 |
| $P$ | | 88 | | 98 | | 98 | | 84 | | 108 | | 92 | | 106 |
| $Q$ | Ti | 2.351 | Ti | 2.367 | Ti | 2.341 | Ti | 2.330 | Zr | 2.134 | Zr | 2.174 | Zr | 2.111 |

[a]Reference 25. [b]Reference 47. [c]Reference 57. [d]Reference 64. [e]Reference 68.

Table 3. The calculated optical bandgaps (in electron volts) for the $SrTiO_3$, $BaTiO_3$, $PbTiO_3$, $BaZrO_3$ and $SrZrO_3$ bulk using different exchange–correlation functionals.

| Crystal | Gap | LDA | PWGGA | PBE | BLYP | B3PW | B3LYP | HF | Exp. |
|---|---|---|---|---|---|---|---|---|---|
| $SrTiO_3$ | Γ–Γ | 2.36[a] | 2.31[a] | 2.35[a] | 2.27[a] | 3.96[a] | 3.89[a] | 12.33[a] | 3.75[b] |
| $BaTiO_3$ | Γ–Γ | 1.98[a] | 1.97[a] | 1.99[a] | 1.91[a] | 3.55[a] | 3.49[a] | 11.73[a] | 3.2[c] |
| $PbTiO_3$ | Γ–Γ | 2.65[a] | 2.61[a] | 2.65[a] | 2.48[a] | 4.32[a] | 4.15[a] | 12.74[a] | 3.4[d] |
| $BaZrO_3$ | Γ–Γ | 3.2[e] | | 3.10[f] | | | 4.79[g] | | 5.0[h] |
| $SrZrO_3$ | Γ–Γ | | 3.53[i] | 3.52[i] | | | 5.31[i] | | 5.6[j] |

[a]Reference 114. [b]Reference 155. [c]Reference 156. [d]Reference 157. [e]Reference 158.
[f]Reference 77. [g]Reference 92. [h]Reference 159. [i]Reference 68. [j]Reference 160.

high degree of $BaTiO_3$ chemical bond covalency, which is typical for all $ABO_3$ perovskites. The bond population between Ti and O atoms in $BaTiO_3$ bulk is exactly the same as in $PbTiO_3$ bulk, namely +98m$e$. The largest bond population between Zr and O atoms is for $BaZrO_3$ bulk, +108m$e$. The smallest bond population between Ti and O atoms between all seven $ABO_3$ perovskites is for the $CaTiO_3$ bulk +84m$e$.

The optical direct (Γ–Γ) bulk bandgaps of five $ABO_3$ perovskites obtained using various functionals are summarized in Table 3. This table clearly demonstrates that pure HF calculations overestimate the optical bandgap several times for all six perovskites, whereas LDA and GGA calculations by factor of approximately 1.5 underestimate it. This tendency is well known in solid state physics for all materials, for example, $CaF_2$ and $BaF_2$.[117,119] The most realistic bandgaps for $SrTiO_3$, $BaTiO_3$, $PbTiO_3$, $BaZrO_3$, $SrZrO_3$ and $PbZrO_3$ perovskites in Refs. 25, 47, 64 and 68 have been obtained using the hybrid B3LYP and B3PW functionals, in agreement with a study by Muscat *et al.*[154]

As we can see from Table 3, the $SrTiO_3$ experimental bandgap is 3.75 eV, as determined by van Benthem *et al.*[155] using the spectroscopic ellipsometry, 3.2 eV bandgap has been experimentally measured for $BaTiO_3$[156] and 3.4 eV for $PbTiO_3$.[157] The calculated optical bandgap for the $SrTiO_3$ perovskite 3.89 eV, using the B3LYP functional in Ref. 114, is in an excellent agreement with the experimental value of 3.75 eV.[155] Using the B3PW hybrid functional,[114] 3.96 eV have been obtained for the $SrTiO_3$ bandgap. The bandgaps calculated for $BaTiO_3$ and $PbTiO_3$ crystals by means of B3LYP functional,[114] 3.49 eV and 4.15 eV, respectively, are also in a satisfactory agreement with the experiment, the discrepancy is 22%. This is acceptable if we take into account the difficulties in determining experimentally the bandgap, including the optical absorption edge tails which extend up to several tenths of eV.[5] The calculated forbidden optical bandgap for the $SrZrO_3$ crystal[68] depends considerably on the choice of the exchange–correlation functional (see Table 3). As usual,[161,162] the HF bandgap is considerably overestimated (13.54 eV), whereas PWGGA (3.53 eV) and PBE (3.52 eV) are underestimated. The best result for the $SrZrO_3$ crystal are obtained for the hybrid B3LYP method.[68] Calculated optical bandgap by means of the B3LYP method,

5.31 eV, is in an excellent agreement with the experimentally measured $SrZrO_3$ optical bandgap of 5.6 eV.[160]

In $ABO_3$ perovskite (001) surface structure simulations presented in Table 4 atoms of two or three outermost surface layers were allowed to relax along the *z*-

Table 4. Calculated atomic relaxation (in percent of bulk lattice constant) for AO and $BO_2$-terminated $ABO_3$ perovskite (001) surfaces. Positive (negative) values refer to displacements outward from (inward to) the surface.

| $SrTiO_3$ | | SrO | termin. | | | | $TiO_2$ | termin. | | |
|---|---|---|---|---|---|---|---|---|---|---|
| Layer | Ion | B3PW[a] | SM[b] | LDA[c] | LDA[d] | Ion | B3PW[a] | SM[b] | LDA[c] | LDA[d] |
| 1 | Sr | −4.84 | −7.10 | −5.7 | −6.66 | Ti | −2.25 | −2.96 | −3.4 | −1.79 |
| | O | 0.84 | 1.15 | 0.1 | 1.02 | O | −0.13 | −1.73 | −1.6 | −0.26 |
| 2 | Ti | 1.75 | 1.57 | 1.2 | 1.79 | Sr | 3.55 | 3.46 | 2.5 | 4.61 |
| | O | 0.77 | 0.87 | 0.0 | 0.26 | O | 0.57 | −0.21 | −0.5 | 0.77 |
| 3 | Sr | | −1.42 | −1.2 | −1.54 | Ti | | −0.60 | −0.7 | −0.26 |
| | O | | 0.70 | −0.1 | 0.26 | O | | −0.29 | −0.5 | 0.26 |
| $BaTiO_3$ | | BaO | termin. | | | $TiO_2$ | termin. | | | |
| Layer | Ion | B3PW[a] | SM[b] | LDA[e] | | Ion | B3PW[a] | SM[b] | LDA[e] | |
| 1 | Ba | −1.99 | −3.72 | −2.79 | | Ti | −3.08 | −2.72 | −3.89 | |
| | O | −0.63 | 1.00 | −1.40 | | O | −0.35 | −0.94 | −1.63 | |
| 2 | Ti | 1.74 | 1.25 | 0.92 | | Ba | 2.51 | 2.19 | 1.31 | |
| | O | 1.40 | 0.76 | 0.48 | | O | 0.38 | −0.17 | −0.62 | |
| 3 | Ba | | −0.51 | 0.53 | | Ti | | −0.33 | −0.75 | |
| | O | | 0.16 | 0.26 | | O | | −0.01 | −0.35 | |
| $PbTiO_3$ | | PbO | termin. | | | | $TiO_2$ | termin. | | |
| Layer | Ion | B3PW[a] | LDA[f] | | | Ion | B3PW[a] | LDA[f] | | |
| 1 | Pb | −3.82 | −4.36 | | | Ti | −2.81 | −3.40 | | |
| | O | −0.31 | −0.46 | | | O | 0.31 | −0.34 | | |
| 2 | Ti | 3.07 | 2.39 | | | Pb | 5.32 | 4.53 | | |
| | O | 2.30 | 1.21 | | | O | 1.28 | 0.43 | | |
| 3 | Pb | | −1.37 | | | Ti | | | −0.92 | |
| | O | | −0.20 | | | O | | −0.27 | | |
| $CaTiO_3$ | | CaO | termin. | | | | $TiO_2$ | termin. | | |
| Layer | Ion | B3PW[g] | GGA[h] | | | Ion | B3PW[g] | GGA[h] | | |
| 1 | Ca | −8.31 | −2.27 | | | Ti | −1.71 | −0.75 | | |
| | O | −0.42 | 0.18 | | | O | −0.10 | −0.13 | | |
| 2 | Ti | 1.12 | 0.70 | | | Ca | 2.75 | 1.98 | | |
| | O | 0.01 | 0.31 | | | O | 1.05 | 0.21 | | |
| 3 | Ca | | −0.82 | | | Ti | | −0.23 | | |
| | O | | −0.03 | | | O | | −0.23 | | |
| $PbZrO_3$ | | PbO | termin. | | | | $ZrO_2$ | termin. | | |
| Layer | Ion | B3LYP[i] | B3PW[j] | LDA[k] | | Ion | B3LYP[i] | B3PW[j] | LDA[k] | |
| 1 | Pb | −5.69 | −6.95 | −4.9 | | Zr | −2.37 | −2.97 | −1.9 | |
| | O | −2.37 | −0.04 | 1.2 | | O | −1.99 | −1.36 | −0.5 | |
| 2 | Zr | 0.57 | 2.57 | 2.6 | | Pb | 4.36 | 5.54 | 4.7 | |
| | O | 0.09 | 1.08 | 0.9 | | O | 1.04 | 0.84 | 1.1 | |
| 3 | Pb | −0.47 | −2.63 | −1.1 | | Zr | −0.47 | −1.12 | −0.3 | |
| | O | −0.47 | −0.26 | 0.3 | | O | −0.28 | −0.53 | 0.3 | |

[a]Reference 25. [b]Reference 44. [c]Reference 42. [d]Reference 41. [e]Reference 46.
[f]Reference 43. [g]Reference 57. [h]Reference 58. [i]Reference 68. [j]Reference 61.
[k]Reference 163.

axis (surfaces of perfect cubic crystals by symmetry have no forces along the $x$- and $y$-axes). A comparison of the surface atomic displacements obtained by different theoretical methods is also done in Table 4. The relaxation of surface metal atoms for $SrTiO_3$, $BaTiO_3$, $PbTiO_3$, $CaTiO_3$ and $PbZrO_3$ perovskite upper two surface layers is much larger than that of oxygen ions what leads to a considerable *rumpling* of the outermost plane (see Tables 4 and 5). The metal atoms of the first and third $SrTiO_3$, $BaTiO_3$, $PbTiO_3$, $CaTiO_3$ and $PbZrO_3$ surface layers relax inwards, i.e., toward the bulk, whereas the second layer metal atoms relax upwards. The only exception is upward relaxation of the BaO-terminated $BaTiO_3$ (001) surface third layer Ba atom obtained by means of the LDA calculations.[46] The CaO-terminated $CaTiO_3$ (001) surface first layer Ca atoms exhibit the strongest relaxation between all AO and $BO_2$-terminated $ABO_3$ perovskite (001) surface atoms. The Ca atom inward relaxation magnitude is 8.31% of the theoretical lattice constant.

In order to compare the calculated surface structures with experimental results, the surface rumpling $s$ (the relative displacement of oxygen with respect to the metal atom in the surface layer) and the changes in interlayer distances $\Delta d_{12}$ and $\Delta d_{23}$ (1, 2 and 3 are the numbers of near-surface layers) are presented in Table 5. Calculations of the interlayer distances are based on the positions of relaxed metal ions, which are known to be much stronger electron scatters than oxygen ions.[7] As

Table 5. Calculated and experimental surface rumpling $s$ and relative displacements of the three near-surface planes for the AO- and $BO_2$-terminated surfaces $\Delta d_{ij}$ (in percent of the lattice constant).

| | | AO-term | | | $BO_2$-term | | |
|---|---|---|---|---|---|---|---|
| | | $s$ | $\Delta d_{12}$ | $\Delta d_{23}$ | $s$ | $\Delta d_{12}$ | $\Delta d_{23}$ |
| $SrTiO_3$ | B3PW[a] | 5.66 | −6.58 | 1.75 | 2.12 | −5.79 | 3.55 |
| | LDA[b] | 5.8 | −6.9 | 2.4 | 1.8 | −5.9 | 3.2 |
| | LDA[c] | 7.7 | −8.6 | 3.3 | 1.5 | −6.4 | 4.9 |
| | SM[d] | 8.2 | −8.6 | 3.0 | 1.2 | −6.4 | 4.0 |
| | LEED[e] | 4.1 ± 2 | −5 ± 1 | 2 ± 1 | 2.1 ± 2 | 1 ± 1 | −1 ± 1 |
| | RHEED[f] | 4.1 | 2.6 | 1.3 | 2.6 | 1.8 | 1.3 |
| $BaTiO_3$ | B3PW[g] | 1.37 | −3.74 | 1.74 | 2.73 | −5.59 | 2.51 |
| | LDA[h] | 1.39 | −3.71 | 0.39 | 2.26 | −5.2 | 2.06 |
| | SM[i] | 0.37 | −2.42 | 2.39 | 1.4 | −6.5 | 3.17 |
| | SM[d] | 4.72 | 4.79 | 1.76 | 1.78 | −4.91 | 2.52 |
| $PbTiO_3$ | B3PW[g] | 3.51 | 6.89 | 3.07 | 3.12 | −8.13 | 5.32 |
| | LDA[j] | 3.9 | 6.75 | 3.76 | 3.06 | −7.93 | 5.45 |
| $CaTiO_3$ | B3PW[h] | 7.89 | −9.43 | 1.12 | 1.61 | −4.46 | 2.75 |
| $PbZrO_3$ | LDA[l] | 6.88 | −8.6 | 3.4 | 1.1 | −7.1 | 4.9 |
| $BaZrO_3$ | B3PW[m] | 3.07 | −4.77 | 0.48 | 0.09 | −3.73 | 1.97 |
| $SrZrO_3$ | B3LYP[n] | 6.77 | −8.49 | 2.39 | −0.72 | −4.19 | 2.85 |
| | LDA[o] | 7.9 | −9.1 | 3.2 | −0.7 | −6.1 | 4.2 |
| | GGA[o] | 7.8 | −9.3 | 3.3 | 0.3 | −7.4 | 4.9 |

[a]Reference 25. [b]Reference 42. [c]Reference 41. [d]Reference 44. [e]Reference 7.
[f]Reference 8. [g]Reference 47. [h]Reference 46. [i]Reference 164. [j]Reference 43.
[k]Reference 57. [l]Reference 63. [m]Reference 64. [n]Reference 68. [o]Reference 65.

we can see from Table 5, nice qualitative agreement, for example for the $SrTiO_3$ perovskite, between all theoretical methods is observed. The amplitude of surface rumpling of SrO-terminated $SrTiO_3$ is predicted to be much larger than that of $TiO_2$-terminated $SrTiO_3$ surface, whereas the rumpling of $BaTiO_3$ $TiO_2$-terminated surface is predicted to exceed by a factor of two that for BaO-terminated surface. In contrast, the $PbTiO_3$ perovskite demonstrates practically equal rumpling for both surface terminations. From Table 5, one can see that all surfaces show the reduction of interlayer distance $d_{12}$ and expansion of $d_{23}$. The calculated surface rumpling agrees quite well with LEED and RHEED experiments[7,8] (which are available so far only for $SrTiO_3$ surfaces). Theory agrees qualitatively also with the LEED results for the $\Delta d_{12}$ and $\Delta d_{23}$. However, the LEED and RHEED experiments demonstrate that the topmost oxygen always move outwards the surfaces whereas all calculations predict for the $TiO_2$-terminated $SrTiO_3$ surface that oxygen goes inwards. Moreover, Table 5 also shows that LEED and RHEED experiments contradict each other in the sign of $\Delta d_{12}$ for SrO-terminated surface and $\Delta d_{23}$ for $TiO_2$-terminated surface. Up to now, the reason for such discrepancies between the different experimental data is not clear and still discussed (e.g., see Ref. 42). Thus, experimental check of our predictions at the moment is prevented by a conflict between different experimental results. New detailed experimental studies are important for resolving this contradiction.

By different methods calculated surface rumpling $s$ for $SrTiO_3$, $BaTiO_3$, $PbTiO_3$, $CaTiO_3$, $BaZrO_3$ and $PbZrO_3$ perovskite (001) surfaces was always positive (see Table 5). In contrast, the *ab initio*[68] calculated surface rumpling for the $ZrO_2$-terminated $SrZrO_3$ (001) surface is negative. Moreover, the calculated negative surface rumpling for the $ZrO_2$-terminated $SrZrO_3$ (001) surface ($-0.72\%$ of $a_0$) is in a surprisingly good agreement with the LDA calculation result by Wang and Arai[65] ($-0.7\%$ of $a_0$), however it is in contrast to the GGA result for the $ZrO_2$-terminated $SrZrO_3$ (001) surface rumpling by the same authors ($+0.3\%$ of $a_0$).

The calculated surface energy for the SrO-terminated $SrTiO_3$ (001) surface[25] by means of hybrid B3PW method is 1.15 eV, which is slightly smaller than the computed surface energy of 1.23 eV for the $TiO_2$ termination (see Table 6). The surface energies for $SrTiO_3$ obtained from the classical shell model[44] (1.32 eV and 1.36 eV for the SrO and $TiO_2$ terminations, respectively) are slightly larger. In contrast to the $SrTiO_3$ (001) surface, we can see that different terminations of the (011) surface lead to large differences in the surface energies. For the $SrTiO_3$ (011) surface, the lowest energy, according to calculations performed in Ref. 25 is 2.04 eV for the O-terminated surface. B3PW calculated surface energy of 3.06 eV for the TiO-terminated $SrTiO_3$ (011) surface is larger than that of the Sr-terminated (011) surface (2.66 eV). The surface energy[90] for Ti-terminated $SrTiO_3$ (111) surface (4.99 eV) is smaller, than the surface energy for $SrO_3$-terminated (111) surface (6.30 eV). The calculated surface energies of the relaxed $BaTiO_3$ (001) and (011) surfaces by means of the hybrid B3PW method[47] and the classical shell model[44] are

Table 6. Calculated surface energies (in eV per surface cell) for $SrTiO_3$, $BaTiO_3$, $PbTiO_3$, $CaTiO_3$, $BaZrO_3$, $SrZO_3$ and $PbZrO_3$ (001), (011) and (111) surfaces with different terminations.

| Crystal | (001) | | (011) | | | (111) | |
|---|---|---|---|---|---|---|---|
| | AO | $BO_2$ | BO | A | O | $AO_3$ | B |
| $SrTiO_3$ | 1.15[a] | 1.23[a] | 3.06[a] | 2.66[a] | 2.04[a] | 6.30[d] | 4.99[d] |
| | 1.32[b] | 1.36[b] | 2.21[b] | 3.04[b] | 1.54[b] | | |
| | | | 2.10[c] | 2.97[c] | 1.40[c] | | |
| $BaTiO_3$ | 1.19[e] | 1.07[e] | 2.04[e] | 3.24[e] | 1.72[e] | 8.40[f] | 7.28[f] |
| | 1.45[b] | 1.40[b] | 2.35[b] | 4.14[b] | 1.81[b] | | |
| $PbTiO_3$ | 0.83[e] | 0.74[e] | 1.36[e] | 2.03[e] | 1.72[e] | | |
| | 0.923[g] | 0.923[g] | 1.834[g] | 1.834[g] | 1.716[g] | | |
| $CaTiO_3$ | 0.94[h] | 1.13[h] | 3.13[h] | 1.91[h] | 1.86[h] | 5.86[i] | 4.18[i] |
| | 0.824[j] | 1.021[j] | 2.180[j] | 1.671[j] | 0.837[j] | 4.49[k] | 3.83[k] |
| $BaZrO_3$ | 1.30[l] | 1.31[l] | 3.09[l] | 2.90[l] | 2.32[l] | 9.33[m] | 7.94[m] |
| $PbZrO_3$ | 1.00[n] | 0.93[n] | 1.89[n] | 1.74[n] | 1.85[n] | | |
| $SrZrO_3$ | 1.13[n] | 1.24[n] | 3.61[n] | 2.21[n] | 2.23[n] | 9.45[o] | 7.98[o] |

[a]Reference 25. [b]Reference 44. [c]Reference 84. [d]Reference 90. [e]Reference 47.
[f]Reference 91. [g]Reference 165. [h]Reference 57. [i]Reference 88. [j]Reference 59.
[k]Reference 87. [l]Reference 64. [m]Reference 92. [n]Reference 68. [o]Reference 93.

presented in Table 6. The B3PW calculated energies for BaO and $TiO_2$-terminated $BaTiO_3$ (001) surfaces (1.19 eV per surface cell) and (1.07 eV per surface cell) demonstrate only a small difference. Unlike the $BaTiO_3$ (001) surface, different terminations of the (011) surface show great differences in the surface energies, according to the calculations performed by means of the B3PW method.[47] The lowest surface energy has the O-terminated surface (1.72 eV). This is close to the energy of $BaTiO_3$ (001) surfaces. That means that O-terminated $BaTiO_3$ (011) surface and $BaTiO_3$ (001) surfaces can co-exist. The Ba-terminated $BaTiO_3$ (011) surface shows much higher surface energy of 3.24 eV, while the $BaTiO_3$ TiO-terminated (011) surface energy is 2.04 eV. Similarly as for the $SrTiO_3$ perovskite, also for $BaTiO_3$, the (111) surface energies are considerably larger than the (001), and even (011) surface energies. The B3LYP calculated[91] surface energy for Ti-terminated $BaTiO_3$ (111) surface is equal to 7.28 eV, while the surface energy for $BaO_3$-terminated $BaTiO_3$ (111) surface is equal to 8.40 eV. The corresponding results are also given for the (001) and (011) surfaces of $PbTiO_3$ in Table 6. B3PW calculations results[47] for the $PbTiO_3$ (001) surfaces are qualitatively similar to those for $BaTiO_3$, although the relaxed surface energies are somewhat lower. For the case of the $PbTiO_3$ (011) surfaces, we find[47] that the surface energy for the O-terminated $PbTiO_3$ (011) surface is exactly the same as for the O-terminated $BaTiO_3$ (011) surface (1.72 eV). It is worth noting, that also the surface energy for the O-terminated $PbTiO_3$ (011) surface (1.716 eV) calculated 2 years later in Ref. 165 practically coincides with the O-terminated $PbTiO_3$ and $BaTiO_3$ (011) surface energy (1.72 eV), calculated in Ref. 47. The surface energies for the $CaTiO_3$ (001) surface[57] are quite similar at 0.94 eV and 1.13 eV, respectively for the CaO and $TiO_2$-terminated surfaces. In con-

trast, different terminations of the (011) $CaTiO_3$ surface lead[57] to very different surface energies of 1.86 eV, 1.91 eV and 3.13 eV for the O-terminated, Ca-terminated and TiO-terminated (011) surface, respectively. B3PW results for $CaTiO_3$ (011) surface energies obtained by Eglitis and Vanderbilt in Ref. 57 contrast sharply with those of Zhang *et al.*,[59] where the authors found a rather different pattern of surface energies. Namely, Zhang *et al.*[59] found that the $TiO_2$-terminated $CaTiO_3$ (001) surface energy 1.021 eV is larger than the O-terminated $CaTiO_3$ (011) surface energy 0.837 eV. This result by Zhang *et al.*[59] for $CaTiO_3$ surfaces contrast sharply with all results of all surface energy calculations for $ABO_3$ perovskites, where the calculated (001) surface energies were always lower than the (011) surface energies. According to my calculations,[64] the $BaZrO_3$ surface energy value for the BaO termination 1.30 eV is slightly smaller than for the $ZrO_2$ termination 1.31 eV. However, the surface energy difference is small, and both surfaces are stable and energetically almost equally favorable. Unlike the $BaZrO_3$ (001) surface,[64] different terminations of the (011) surface lead to great differences in the surface energies. The lowest calculated energy is that of the O-terminated $BaZrO_3$ (011) surface 2.32 eV. In Ref. 64 calculated surface energy for the ZrO-terminated $BaZrO_3$ (011) surface 3.09 eV is larger than that for the Ba-terminated $BaZrO_3$ (011) surface 2.90 eV. The B3LYP calculated[92] surface energy for Zr-terminated $BaZrO_3$ (111) surface is equal to 7.94 eV, while the surface energy for $BaO_3$-terminated (111) surface is equal to 9.33 eV.

The atomic displacements $D$, effective static atomic charges $Q$, and bond populations $P$ between nearest metal and oxygen atoms for the $SrTiO_3$, $BaTiO_3$ and $PbTiO_3$ (001) surfaces are given[25,47] in Table 7. The major effect observed here for all three $SrTiO_3$, $BaTiO_3$ and $PbTiO_3$ perovskites is a strengthening of the Ti–O chemical bond near the $TiO_2$-terminated (001) surface. It is interesting to note, that the Ti and O effective charges in bulk $SrTiO_3$ of $2.351e$ and $-1.407e$, in bulk $BaTiO_3$ of $2.367e$ and $-1.388e$ and in bulk $PbTiO_3$ of $2.341e$ and $-1.232e$, respectively (see Table 2), are much smaller than those expected in an ionic model ($4e$ and $-2e$, respectively). The Ti–O bond population for the $TiO_2$-terminated $SrTiO_3$ (001) surface is $0.118e$, as well as $0.126e$ and $0.114e$ for the $TiO_2$-terminated $BaTiO_3$ and $PbTiO_3$ (001) surfaces (see Table 7), which is considerably larger than the respective values of $0.088e$, $0.098e$ and $0.098e$ in the $SrTiO_3$, $BaTiO_3$ and $PbTiO_3$ bulk.[25,47] In contrast, the Sr–O and Ba–O bond populations are very small. The lack of covalency in the Sr–O and Ba–O bonds are also seen in the Sr and Ba effective charges of $1.871e$ and $1.797e$ in the bulk and $1.846e$ and $1.752e$ on the SrO- and the BaO-terminated (001) surface, which are close to the formal ionic charge of $2e$.

The optical bandgaps for $SrTiO_3$, $BaTiO_3$, $PbTiO_3$, $SrZrO_3$ and $BaZrO_3$ perovskites surfaces and bulk as calculated by means of the hybrid DFT technique are presented in Table 8. One can see good agreement between the theory and experiment. We should stress here the remarkable agreement of the bulk bandgap with

Table 7. Calculated absolute magnitudes of atomic displacements $D$ (in Å), the effective atomic charges $Q$ (in $e$), and the bond populations $P$ between nearest Me–O atoms (in $e$) for the $TiO_2$, SrO, BaO and PbO-terminated $SrTiO_3$, $BaTiO_3$ and $PbTiO_3$ (001) surfaces.

| | | STO | | | | BTO | | | | PTO | | |
|---|---|---|---|---|---|---|---|---|---|---|---|---|
| Layer | Prop | Ion | $TiO_2$ | Ion | SrO | Ion | $TiO_2$ | Ion | BaO | Ion | $TiO_2$ | Ion | PbO |
| 1 | $D$ | Ti | −0.088[a] | Sr | −0.189 | Ti | −0.123[b] | Ba | −0.080 | Ti | −0.111[b] | Pb | −0.150 |
| | $Q$ | | 2.291 | | 1.846 | | 2.307 | | 1.752 | | 2.279 | | 1.276 |
| | $P$ | | 0.118 | | −0.006 | | 0.126 | | −0.030 | | 0.114 | | 0.054 |
| | $D$ | O | −0.005 | O | 0.033 | O | −0.014 | O | −0.025 | O | 0.012 | O | −0.012 |
| | $Q$ | | −1.296 | | −1.522 | | −1.280 | | −1.473 | | −1.184 | | −1.128 |
| | $P$ | | −0.014 | | 0.074 | | −0.038 | | 0.080 | | 0.044 | | 0.106 |
| 2 | $D$ | Sr | 0.139 | Ti | 0.068 | Ba | 0.101 | Ti | 0.070 | Pb | 0.209 | Ti | 0.121 |
| | $Q$ | | 1.850 | | 2.363 | | 1.767 | | 2.379 | | 1.275 | | 2.331 |
| | $P$ | | −0.008 | | 0.078 | | −0.030 | | 0.088 | | 0.008 | | 0.080 |
| | $D$ | O | 0.022 | O | 0.030 | O | 0.015 | O | 0.056 | O | 0.050 | O | 0.091 |
| | $Q$ | | −1.365 | | −1.450 | | −1.343 | | −1.418 | | −1.167 | | −1.258 |
| | $P$ | | 0.080 | | −0.010 | | 0.090 | | −0.030 | | 0.080 | | 0.006 |
| 3 | $Q$ | Ti | 2.348 | Sr | 1.875 | Ti | 2.365 | Ba | 1.803 | Ti | 2.335 | Pb | 1.358 |
| | $P$ | | 0.096 | | −0.012 | | 0.104 | | −0.036 | | 0.108 | | 0.024 |
| | $Q$ | O | −1.384 | O | −1.429 | O | −1.371 | O | −1.417 | O | −1.207 | O | −1.259 |
| | $P$ | | −0.010 | | 0.084 | | −0.034 | | 0.098 | | 0.018 | | 0.096 |

[a]Reference 25. [b]Reference 47.

Table 8. Calculated optical bandgap for $SrTiO_3$, $BaTiO_3$, $PbTiO_3$ (001), as well as for $SrZrO_3$ (001) and (011) and $BaZrO_3$ (111) surfaces (in eV).

| Term | STOgap | Term | BTOgap | Term | PTOgap | Term | SZOgap | Term | BZOgap |
|---|---|---|---|---|---|---|---|---|---|
| Exp. | 3.75[a] | Exp. | 3.2[c] | Exp. | 3.4[d] | Exp. | 5.6[e] | Exp. | 5.00[g] |
| Bulk | 3.96[b] | Bulk | 3.55[b] | Bulk | 4.32[b] | Bulk | 5.31[f] | Bulk | 4.79[h] |
| SrO (001) | 3.72[b] | BaO (001) | 3.49[b] | PbO (001) | 3.58[b] | SrO (001) | 5.04[f] | $BaO_3$ (111) | 4.51[h] |
| $TiO_2$ (001) | 3.95[b] | $TiO_2$ (001) | 2.96[b] | $TiO_2$ (001) | 3.18[b] | $ZrO_2$ (001) | 4.91[f] | Zr (111) | 4.47[h] |
| | | | | | | O (011) | 5.27[f] | | |
| | | | | | | Sr (011) | 4.40[f] | | |
| | | | | | | ZrO (011) | 5.07[f] | | |

[a]Reference 155. [b]Reference 32. [c]Reference 156. [d]Reference 157. [e]Reference 160. [f]Reference 68. [g]Reference 159. [h]Reference 92.

the experiment for $SrTiO_3$ (3.96 eV versus 3.75 eV) and for $BaZrO_3$ (4.79 eV versus 5.00 eV). This is in a sharp contrast with the typical HF overestimate of the gap and DFT underestimate for oxide and fluoride materials[114,119,166–168] (e.g., 1.8 eV for $SrTiO_3$ and $BaTiO_3$[42,46]).

The optical bandgap for the SrO- and $TiO_2$-terminated $SrTiO_3$ (001) surface becomes smaller with respect to the bulk bandgap.[32] In the Ref. 32 by means of the hybrid B3PW method calculated bulk optical bandgap (3.96 eV) is considerably reduced for the SrO-terminated (3.72 eV) $SrTiO_3$ (001) surface. In contrast, the optical bandgap for the $TiO_2$-terminated $SrTiO_3$ (001) surface (3.95 eV) is only slightly, by 0.01 eV, reduced with respect to the bulk value.[32] According to the earlier LDA calculations[42] by Padilla and Vanderbilt performed 15 years ago for the $SrTiO_3$ (001) surface, we see that the bandgap for the SrO-terminated surface (1.86 eV) almost does not change with respect to the bulk value (1.85 eV). For the $TiO_2$-terminated surface, there is a substantial reduction of the bandgap (1.13 eV).

The $BaTiO_3$ bulk bandgap[46] calculated by Padilla and Vanderbilt by means of the LDA method is 1.79 eV, to be compared with the experimental value of 3.2 eV; this level of disagreement is typical for the LDA. The calculated[46] LDA band structure for cubic BaO-terminated $BaTiO_3$ (001) surface shows, that the bulk gap (1.79 eV) is slightly increased (1.80 eV) near the BaO-terminated (001) surface. On the $TiO_2$-terminated $BaTiO_3$ (001) surface, however, the bandgap is very strongly reduced (0.84 eV).[46] According to the B3PW calculations performed in Ref. 34, the $BaTiO_3$ optical bulk bandgap (3.55 eV) is in a good agreement with the experimental value of (3.2 eV). The optical bandgap near the BaO-terminated (3.49 eV) and $TiO_2$-terminated (2.96 eV) $BaTiO_3$ (001) surfaces are reduced with respect to the bulk value (see Table 8). By means of the hybrid B3PW method calculated[32] bulk bandgap for $PbTiO_3$ (4.32 eV) by 0.92 eV exceed the experimental value (3.4 eV). The calculated bandgaps[32] of PbO (3.58 eV) and $TiO_2$ (3.18 eV) terminated $PbTiO_3$ (001) surface are strongly, by 0.74 eV and 1.14 eV reduced with respect to the $PbTiO_3$ bulk bandgap value.

We should stress here outstanding agreement of in Ref. 68 by means of the B3LYP method calculated $SrZrO_3$ optical bulk bandgap, 5.31 eV, with the experimental value of 5.6 eV (see Table 8). This is in a sharp contrast with the typical HF overestimate of the optical bulk bandgap, 13.54 eV, and PBE underestimate of 3.52 eV.[68] The calculated optical bandgap for the SrO (5.04 eV) and $ZrO_2$ (4.91 eV) terminated $SrZrO_3$ surfaces becomes smaller with respect to the bulk optical bandgap (5.31 eV).[68] By means of the hybrid B3LYP method calculated[92] $BaZrO_3$ optical bulk band gap (4.79 eV) is very slightly underestimated by 4% (see Table 8) regarding the experimental value of (5.00 eV). The calculated optical band gap near the Zr- and $BaO_3$-terminated $BaZrO_3$ (111) surfaces is reduced by approximately 6% with respect to the bulk value. The B3LYP calculated optical bandgap values for Zr- and $BaO_3$-terminated $BaZrO_3$ (111) surfaces are very close and differ only by 0.04 eV.[92]

Table 9. Atomic relaxation of the $SrTiO_3$, $BaTiO_3$, $PbTiO_3$ and $CaTiO_3$ (011) surfaces (in percent of the bulk lattice constant) for the three terminations calculated by means of the *ab initio* B3PW method and classical SM. A positive sign corresponds to outward atomic displacements (toward the vacuum).

| | | $SrTiO_3$ | | | $BaTiO_3$ | | | $PbTiO_3$ | | | $CaTiO_3$ | |
|---|---|---|---|---|---|---|---|---|---|---|---|---|
| Layer | Ion | $\Delta z$ | $\Delta y$ | Ion | $\Delta z$ | $\Delta y$ | Ion | $\Delta z$ | $\Delta y$ | Ion | $\Delta z$ | $\Delta y$ |
| | | TiO-term | | | TiO-term | | | TiO-term | | | TiO-term | |
| 1 | Ti | −7.69[a] | — | Ti | −6.93[b] | — | Ti | −8.13[c] | — | Ti | −7.14[d] | — |
| 1 | O | 3.59 | — | O | 6.45 | — | O | 3.30 | — | O | 4.67 | — |
| 2 | O | −0.51 | — | O | −1.66 | — | O | −0.41 | — | O | −0.44 | — |
| 3 | Sr | −2.10 | — | Ba | −3.85 | — | Pb | −2.54 | — | Ca | −2.75 | — |
| 3 | O | −2.56 | — | O | −2.40 | — | O | −4.07 | — | O | −3.79 | — |
| 3 | Ti | 0.16 | — | Ti | 1.59 | — | Ti | 0.30 | — | Ti | −0.78 | — |
| | | Sr-term | | | Ba-term | | | Pb-term | | | Ca-term | |
| 1 | Sr | −12.81[a] | — | Ba | −13.49[b] | — | Pb | −11.94[c] | — | Ca | −16.05[d] | — |
| 2 | O | 1.02 | — | O | 2.80 | — | O | −0.61 | — | O | 1.35 | — |
| 3 | Ti | −0.04 | — | Ti | −1.20 | — | Ti | 1.78 | — | Ti | −0.37 | — |
| 3 | O | −1.08 | — | O | −2.94 | — | O | 1.67 | — | O | −1.71 | — |
| 3 | Sr | 0.26 | — | Ba | 2.52 | — | Pb | 1.52 | — | Ca | −0.93 | — |
| | | O-term | | | O-term | | | O-term | | | O-term | |
| 1 | O | −6.61[a] | −0.14[a] | O | −11.16[b] | −6.70[b] | O | −7.37[c] | −0.07[c] | O | −6.10[d] | −2.16[d] |
| 2 | Ti | −1.02 | −4.35 | Ti | −1.83 | −5.33 | Ti | 0.20 | −2.54 | Ti | −0.26 | −4.70 |
| 2 | Sr | −1.18 | 0.85 | Ba | 4.84 | −2.21 | Pb | 0.18 | −7.50 | Ca | −2.10 | −0.27 |
| 2 | O | 1.79 | 6.40 | O | 4.54 | 5.90 | O | 0.51 | 2.19 | O | 3.43 | 8.05 |
| 3 | O | −0.79 | 2.10 | O | 6.52 | 5.58 | O | −0.41 | 3.30 | O | −0.55 | 1.90 |

[a]Reference 25. [b]Reference 44. [c]Reference 47. [d]Reference 57.

### 3.2. *$ABO_3$ perovskite (011) and (111) surface structure*

Table 9 for the $SrTiO_3$, $BaTiO_3$, $PbTiO_3$ and $CaTiO_3$ (011) surfaces is similar to Table 4 for the corresponding (001) surfaces, whereas Table 10 complements these data by the predicted surface rumpling and the relative displacements of the two top layers. For the TiO-terminated surface, the rumpling for all four $SrTiO_3$, $BaTiO_3$, $PbTiO_3$ and $CaTiO_3$ (011) surfaces is qualitatively similar and really huge, ≈ 10–14%. For all four calculated $ABO_3$ perovskites, this arise due to a combination of a strong O ion outward displacement by (3–6%) and large Ti ion inward displacement by approximately (7–8%). This calculated surface rumpling is much larger than that found for the (001) surface. The reduction of relative distances between the first and second layer for TiO-terminated (011) surface for all four calculated perovskites (see Table 10) are in the range between (4%) and (7%). This reduction of interlayer distance between the first and the second layer is considerably larger than the reduction of the interlayer distance between the second and the third layer. As we can see from the Table 10, the TiO-terminated $CaTiO_3$ (001) surface, in contrast to $SrTiO_3$, $BaTiO_3$ and $PbTiO_3$ perovskites, shows expansion between the second and third layers.

On the Sr, Ba, Pb and Ca-terminated $SrTiO_3$, $BaTiO_3$, $PbTiO_3$ and $CaTiO_3$ (011) surfaces, the upper layer Sr, Ba, Pb and Ca atoms move very strongly inwards

Table 10. Surface rumpling $s$ and relative displacements $\Delta d_{ij}$ (in percent of the bulk lattice constant) for three near-surface planes of the TiO and O-terminated $SrTiO_3$, $BaTiO_3$, $PbTiO_3$ and $CaTiO_3$ (011) surface.

| | | TiO-term | | O-term | |
|---|---|---|---|---|---|
| $SrTiO_3$ | $s$ | $\Delta d_{12}$ | $\Delta d_{23}$ | $\Delta d_{12}$ | $\Delta d_{23}$ |
| B3PW[a] | 11.28 | −7.18 | −0.67 | −5.59 | −0.23 |
| SM[b] | 14.47 | −4.27 | −3.86 | −11.83 | 8.69 |
| $BaTiO_3$ | | | | | |
| B3PW[c] | 10.47 | −6.84 | −1.02 | −5.25 | −1.05 |
| SM[b] | 13.38 | −5.27 | −3.25 | −9.33 | −8.35 |
| $PbTiO_3$ | | | | | |
| B3PW[c] | 11.43 | −4.83 | −0.71 | −7.57 | −5.84 |
| $CaTiO_3$ | | | | | |
| B3PW[d] | 11.81 | −6.70 | 2.31 | −5.84 | 0.29 |

[a]Reference 25. [b]Reference 44. [c]Reference 47. [d]Reference 57.

by 12.81, 13.49, 11.94 and 16.05% of the lattice constant $a_0$, respectively (see Table 9). These Sr, Ba, Pb and Ca atomic displacement magnitudes are the largest atomic displacement magnitudes among all in Table 9 calculated $SrTiO_3$, $BaTiO_3$, $PbTiO_3$ and $CaTiO_3$ (011) surface atoms. The second layer O atoms for the Sr, Ba and Ca-terminated $SrTiO_3$, $BaTiO_3$ and $CaTiO_3$ (011) surfaces relax outwards by 1.02, 2.80 and 1.35% of $a_0$, respectively, whereas the Pb-terminated $PbTiO_3$ (011) surface second layer O atom relax inwards by 0.61% of $a_0$ (see Table 9). The third layer atoms for the Sr, Ba and Ca-terminated $SrTiO_3$, $BaTiO_3$ and $CaTiO_3$ (011) surfaces relax inwards. The only two exceptions there are the outward movement of the Sr-terminated $SrTiO_3$ (011) surface third layer Sr atom (0.26%), and rather strong Ba-terminated $BaTiO_3$ (011) surface third layer Ba atom displacement by 2.52% of $a_0$ (see Table 9). In contrast to Sr, Ba and Ca-terminated $SrTiO_3$, $BaTiO_3$ and $CaTiO_3$ (011) surfaces, all Pb-terminated $PbTiO_3$ (011) surface third layer atoms relax outwards. For the O-terminated $SrTiO_3$, $BaTiO_3$, $CaTiO_3$ and $PbTiO_3$ (011) surface (see Table 9), the upper layer O atom displacement directions along the $z$- and $y$-axes are the same for all four perovskites. Nevertheless, the displacement magnitudes of the upper layer O atom are quite different for different perovskites. As we can see from Table 9, the atomic displacements in the third plane from the surface for all three terminations of the $SrTiO_3$, $BaTiO_3$, $PbTiO_3$ and $CaTiO_3$ (011) surface are still large. This is in sharp contrast to results for the neutral (001) surfaces in Table 4, where the atomic displacements converged very quickly and were already negligible in the third layer.

Table 11 shows the calculated Mulliken effective charges $Q$ and their changes $\Delta Q$ with respect to bulk $SrTiO_3$, $BaTiO_3$, $PbTiO_3$ and $CaTiO_3$ for the three (011) terminations in Ref. 25, 47 and 57. The charge of the surface Ti atoms in the TiO-terminated $SrTiO_3$, $BaTiO_3$, $PbTiO_3$ and $CaTiO_3$ (011) surface is reduced by $0.14e$, $0.151e$, $1.129e$ and $0.126e$, respectively. Metal atoms in the third layer lose much

Table 11. Calculated Mulliken atomic charges $Q$ (in $e$) and changes in atomic charges $\Delta Q$ with respect to the bulk charges (in $e$) for the three $SrTiO_3$, $BaTiO_3$, $PbTiO_3$ and $CaTiO_3$ (011) surface terminations.

| Atom | $Q$ | $\Delta Q$ | Atom | $Q$ | $\Delta Q$ | Atom | $Q$ | $\Delta Q$ | Atom | $Q$ | $\Delta Q$ |
|---|---|---|---|---|---|---|---|---|---|---|---|
| $SrTiO_3$ | TiO-term | | $BaTiO_3$ | TiO-term | | $PbTiO_3$ | TiO-term | | $CaTiO_3$ | TiO-term | |
| Ti(I) | 2.211[a] | −0.140[a] | Ti(I) | 2.216[b] | −0.151[b] | Ti(I) | 2.212[b] | −0.129[b] | Ti(I) | 2.204[c] | −0.126[c] |
| O(I) | −1.305 | 0.102 | O(I) | −1.316 | 0.072 | O(I) | −1.261 | −0.029 | O(I) | −1.290 | 0.081 |
| O(II) | −1.160 | 0.247 | O(II) | −1.155 | 0.233 | O(II) | −1.057 | 0.175 | O(II) | −1.139 | 0.232 |
| Sr(III) | 1.843 | −0.028 | Ba(III) | 1.757 | −0.04 | Pb(III) | 1.253 | −0.101 | Ca(III) | 1.733 | −0.049 |
| Ti(III) | 2.333 | −0.018 | Ti(III) | 2.353 | −0.014 | Ti(III) | 2.328 | −0.013 | Ti(III) | 2.309 | −0.021 |
| O(III) | −1.333 | 0.074 | O(III) | −1.299 | 0.089 | O(III) | −1.18 | 0.052 | O(III) | −1.302 | 0.069 |
| O(IV) | −1.429 | −0.022 | O(IV) | −1.402 | −0.014 | O(IV) | −1.239 | −0.007 | O(IV) | −1.375 | −0.004 |
| | Sr-term | | | Ba-term | | | Pb-term | | | Ca-term | |
| Sr(I) | 1.766 | −0.105 | Ba(I) | 1.636 | −0.161 | Pb(I) | 1.122 | −0.232 | Ca(I) | 1.676 | −0.106 |
| O(II) | −1.560 | −0.153 | O(II) | −1.483 | −0.095 | O(II) | −1.140 | 0.092 | O(II) | −1.488 | −0.117 |
| Sr(III) | 1.874 | 0.003 | Ba(III) | 1.799 | 0.002 | Pb(III) | 1.340 | −0.014 | Ca(III) | 1.781 | −0.001 |
| Ti(III) | 2.362 | 0.011 | Ti(III) | 2.368 | 0.001 | Ti(III) | 2.343 | 0.002 | Ti(III) | 2.334 | 0.004 |
| O(III) | −1.486 | −0.079 | O(III) | −1.446 | −0.058 | O(III) | −1.277 | −0.045 | O(III) | −1.452 | −0.081 |
| O(IV) | −1.396 | 0.011 | O(IV) | −1.392 | −0.004 | O(IV) | −1.247 | −0.015 | O(IV) | −1.363 | 0.008 |
| | O-term | | | O-term | | | O-term | | | O-term | |
| O(I) | −1.172 | 0.235 | O(I) | −1.158 | 0.23 | O(I) | −1.011 | 0.221 | O(I) | −1.139 | 0.232 |
| Sr(II) | 1.851 | −0.020 | Ba(II) | 1.766 | −0.031 | Pb(II) | 1.257 | −0.097 | Ca(II) | 1.751 | −0.031 |
| Ti(II) | 2.240 | −0.111 | Ti(II) | 2.213 | −0.154 | Ti(II) | 2.237 | −0.104 | Ti(II) | 2.235 | −0.095 |
| O(II) | −1.461 | −0.054 | O(II) | −1.452 | −0.064 | O(II) | −1.261 | −0.029 | O(II) | −1.422 | −0.051 |
| O(III) | −1.394 | 0.013 | O(III) | −1.317 | 0.071 | O(III) | −1.215 | 0.017 | O(III) | −1.359 | 0.012 |
| Sr(IV) | 1.867 | −0.004 | Ba(IV) | 1.792 | −0.005 | Pb(IV) | 1.355 | 0.001 | Ca(IV) | 1.774 | −0.008 |
| Ti(IV) | 2.332 | −0.019 | Ti(IV) | 2.317 | −0.05 | Ti(IV) | 2.317 | −0.024 | Ti(IV) | 2.310 | −0.020 |
| O(IV) | −1.433 | −0.026 | O(IV) | −1.407 | −0.019 | O(IV) | −1.233 | −0.001 | O(IV) | −1.398 | −0.027 |

[a]Reference 25. [b]Reference 47. [c]Reference 57.

less charge, with Sr and Ti atoms losing 0.028$e$ and 0.018$e$, respectively in $SrTiO_3$. Ba, Pb and Ca atoms lose 0.04$e$, 0.101$e$ and 0.049$e$, as well as Ti atoms lose 0.014$e$, 0.013$e$ and 0.021$e$ in $BaTiO_3$, $PbTiO_3$ and $CaTiO_3$ perovskites, respectively (see Table 11). The $SrTiO_3$, $BaTiO_3$ and $CaTiO_3$ TiO-terminated (011) surface O ions in the first, second and third layers, except the central one, also have charges that are reduced by 0.102$e$, 0.247$e$, and 0.074$e$ for $SrTiO_3$, by 0.072$e$, 0.233$e$ and 0.089$e$ for $BaTiO_3$ and by 0.081e, 0.232e and 0.069e for $CaTiO_3$, respectively (i.e., they become less negative). In contrast, in all four in Table 11 analyzed perovskites, the central-layer O-ions slightly increase their charges by 0.022$e$, 0.014$e$, 0.007$e$ and 0.004$e$, respectively. The largest charge change in $SrTiO_3$, $BaTiO_3$, $PbTiO_3$ and $CaTiO_3$ perovskites is observed for subsurface O atoms (0.247$e$, 0.233$e$, 0.175$e$ and 0.232$e$, respectively), which add up to contribute a large positive change of 0.494$e$, 0.466$e$, 0.350$e$ and 0.464$e$, respectively in the subsurface layer.

The analysis of the interatomic bond populations for the three possible $SrTiO_3$, $BaTiO_3$, $PbTiO_3$ and $CaTiO_3$ (011) surface terminations shows, that the most important effect observed here is a strong increase in the Ti–O chemical bonding near the surface as compared to already large Ti–O bonding in the bulk for all four perovskites.[25,47,57] The most significant increase in the Ti–O chemical bonding in $SrTiO_3$, $BaTiO_3$, $PbTiO_3$ and $CaTiO_3$ perovskites occurs near the TiO-terminated (011) surface (0.130$e$, 0.130$e$, 0.132$e$ and 0.128$e$, respectively), which is much stronger than the relevant Ti–O chemical bonding value near the $TiO_2$-terminated (001) surface (0.118$e$, 0.126$e$, 0.114$e$ and 0.114$e$, respectively) and in the bulk (0.088$e$, 0.098$e$, 0.098$e$ and 0.084$e$, respectively).

According to the results of the calculations for $SrTiO_3$ (111) surfaces,[89] the upper layer Ti atom for Ti-terminated $SrTiO_3$ (111) surface strongly (by 3.58% of the bulk lattice constant $a_0$) relaxes inwards (see Table 12). The second layer Sr

Table 12. Calculated relaxation of Ti and $SrO_3$-terminated $SrTiO_3$ (111), Zr and $BaO_3$-terminated $BaZrO_3$ (111) and Zr- and $SrO_3$-terminated $SrZrO_3$ (111) surface upper three layer atoms (as a percentage of the bulk crystal lattice constant $a_o = 3.914$ Å, $a_o = 4.234$ Å and $a_o = 4.195$ Å, respectively).

| | $SrTiO_3$ | | | $BaZrO_3$ | | | $SrZrO_3$ | |
|---|---|---|---|---|---|---|---|---|
| Layer | Ion | $\Delta z$ | Layer | Ion | $\Delta z$ | Layer | Ion | $\Delta z$ |
| | Ti-term | | | Zr-term | | | Zr-term | |
| 1 | Ti | −3.58[a] | 1 | Zr | −8.03[b] | 1 | Zr | −5.72[c] |
| 2 | Sr | −11.24 | 2 | Ba | −9.73 | 2 | Sr | −11.92 |
| 2 | O | 1.53 | 2 | O | 0.78 | 2 | O | 0.79 |
| 3 | Ti | 0.26 | 3 | Zr | −0.02 | 3 | Zr | 1.53 |
| | $SrO_3$-term | | | $BaO_3$-term | | | $SrO_3$-term | |
| 1 | Sr | 1.33[a] | 1 | Ba | 1.70[b] | 1 | Sr | −0.74[c] |
| 1 | O | −0.03 | 1 | O | −0.57 | 1 | O | −0.52 |
| 2 | Ti | 1.81 | 2 | Zr | 0.21 | 2 | Zr | 0.74 |
| 3 | Sr | −0.03 | 3 | Ba | 0.71 | 3 | Sr | −0.02 |
| 3 | O | −0.26 | 3 | O | −0.01 | 3 | O | −0.18 |

[a]Reference 89. [b]Reference 92. [c]Reference 93.

atom moves inwards by huge magnitude of 11.24% of $a_0$, while the second layer O atom relaxes outwards by 1.53% of $a_0$. Outward displacement of the third layer Ti atom is rather weak, less than 1% of $a_0$. For the $SrO_3$-terminated $SrTiO_3$ (111) surface, the upper layer metal atom moves outwards by 1.33% of $a_0$, but the upper layer O atom is displaced very slightly inwards by 0.03% of $a_0$. The second layer Ti atom outward displacement (1.81% of $a_0$) is larger than the upper layer Sr atom relaxation. Both third layer Sr and O atoms move inwards by a very small magnitude (0.03% of $a_0$ and 0.26% of $a_0$), respectively (see Table 12). The calculated surface relaxation energy for Ti-terminated $SrTiO_3$ (111) surface (−1.66 eV) is almost five times larger, than the surface relaxation energy for $SrO_3$-terminated $SrTiO_3$ (111) surface[89] (−0.35 eV).

The upper layer Zr atom for Zr-terminated $BaZrO_3$ (111) surface strongly (by 8.03% of bulk lattice constant $a_0$) moves inwards toward the bulk (see Table 12).[92] The second layer Ba atom moves inwards even more strongly (by 9.73% of $a_0$), while the second layer O atom relaxes slightly outwards by 0.78% of $a_0$. Inward relaxation of the third layer Zr atom is very weak, only 0.02% of $a_0$ (see Table 12). For the $BaO_3$-terminated $BaZrO_3$ (111) surface the upper layer metal and oxygen atoms relax outwards and inwards by 1.70% of $a_0$ and 0.57% of $a_0$, respectively.[92] The second layer Zr atom outward relaxation magnitude (0.21% of $a_0$) is smaller than the third layer metal atom displacement magnitude. The calculated surface relaxation energy for Zr-terminated $BaZrO_3$ (111) surface (−1.49 eV) is almost fifteen times larger than the surface relaxation energy for $BaO_3$-terminated $BaZrO_3$ (111) surface (−0.10 eV).

According to the results of calculations performed in Ref. 93, the upper layer Zr atom for Zr-terminated $SrZrO_3$ (111) surface strongly relaxes inwards toward the bulk (by 5.72% of $a_0$) (see Table 12). The second layer Sr atom relaxes inwards even more strongly (by 11.92% of $a_0$), while the second layer O atom relaxes outwards by 0.79% of $a_0$. Outward relaxation of the third layer Zr atom, similarly to the $SrTiO_3$ and $BaZrO_3$ perovskites, again is rather weak, only 1.53% of $a_0$. For the $SrO_3$-terminated $SrZrO_3$ (111) surface the upper layer metal atom and oxygen atoms moves inwards by 0.74% and 0.52% of $a_0$, respectively. The second layer Zr atom outward relaxation magnitude (0.74% of $a_0$) is exactly the same as the upper layer Sr atom inward relaxation. Both third layer Sr and O atoms relax inwards by a very small magnitude (0.02% of $a_0$ and 0.18% of $a_0$), respectively. Again, typically for $ABO_3$ perovskite (111) surfaces, the calculated surface relaxation energy for Zr-terminated $SrZrO_3$ (111) surface (−1.57 eV) is almost sixteen times larger, than the surface relaxation energy for $SrO_3$-terminated $SrZrO_3$ (111) surface[93] (−0.10 eV).

### 3.3. *Ab initio calculations of Nb impurity in $SrTiO_3$*

The calculated[106] average Sr charges in the 3 × 3 × 3 times extended $SrTiO_3$ supercell are $1.92e$, very close to the formal ionic charge of $+2e$. This is in a sharp contrast with Ti ions ($2.77e$) and O ions ($-1.57e$), which indicates high degree of

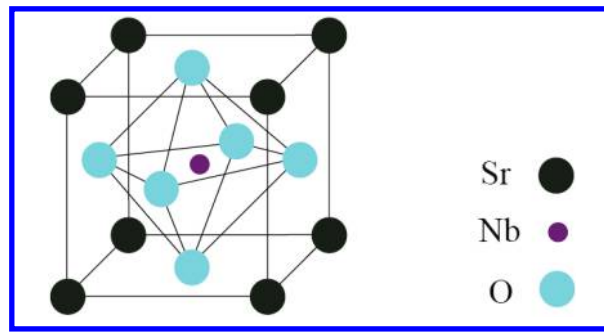


Fig. 5. Sketch of Nb doped $SrTiO_3$ crystal.

Table 13. Calculated Mulliken bond populations $P$ (me) between different atoms in Nb doped $SrTiO_3$ crystal using $3 \times 3 \times 3$ times extended $SrTiO_3$ supercells containing 135 atoms.

| Atom A | Atom B | $P$ (me) | $R$ (Å) |
|---|---|---|---|
| Nb | O | 8[a] | 1.995 |
| Ti | O | 64 | 1.945 |
| Sr | O | −22 | 2.751 |
| Sr | Ti | 0 | 3.369 |
| Sr | Nb | 0 | 3.369 |

[a]Reference 106.

covalency of the chemical bonding. For a single Nb ion, which replaces the Ti ion (see Fig. 5), the effective charge of $3.13e$ were found. This charge difference between the Ti and Nb ions ($0.36e$) is donated mainly to six nearest O ions which become more negative.

According to the results of our calculations, six nearest oxygen atoms are symmetrically slightly repulsed from the Nb impurity by 0.05 Å.[106] It is worth noting, that Hamid in Ref. 169 using the LDA approximation got just opposite result for 6 O atoms relaxation. According to the LDA calculations by Hamid,[169] the six nearest O neighbors show inward relaxation toward the Nb impurity, along the ⟨001⟩ direction by 0.09 Å. The calculated[106] bond populations between the nearest Ti and O atoms indicate considerable covalency effect[170,171] (see Table 13). Just opposite, the calculated bond population between the nearest Nb and O ions turns out to be much smaller, 8 versus 64 me for the Ti–O bond. This is caused by more ionic charges of Nb and nearest O as compared to Ti and nearest O ions. The bond populations between nearest Sr and O atoms are negative which indicates the lack of chemical interaction between these ions.

The calculated HF optical bandgap is as usually strongly overestimated 12.5 eV.[106] The Nb impurity band in HF calculations is located 1.13 eV below the conduction band bottom. If we scale the HF calculated $SrTiO_3$ band gap down to the experimental value, the Nb state would be located approximately 0.25 eV

below the CB bottom, which means that Nb impurity in $SrTiO_3$ is a shallow donor. Figure 2 in Ref. 106 shows the electronic charge density map of Nb doped $SrTiO_3$ bulk (the (001) plane). This figure confirms the population analysis about the covalent chemical bonding and larger effective charge of Nb ion compared to the host Ti ion.

### 3.4. *Computer modeling of F centers in $KNbO_3$, $PbZrO_3$, $SrTiO_3$ and $PbTiO_3$*

One of the most common defects in $ABO_3$ perovskite crystals is the so-called $F$ center, an O vacancy $V_O$ which traps two electrons (see Fig. 6). First principles calculations of the $F$ centers in $KNbO_3$ were performed already 16 years ago by Eglitis *et al.*[108] using the LMTO method combined with DFT (local approximation) and the method of the INDO and relatively small 40 atom supercells. These LMTO calculations have shown for the first time that even in the ground state of the $F$ center, the two electrons from the missing anion are considerably delocalized over the two nearest Nb ions, and only 0.6 electrons are inside the O vacancy sphere, very close to the result of INDO calculation for the relaxed structure.[108,172–174] The INDO optimized atomic relaxation around the $F$ center in $KNbO_3$ indicates a strong outward shift of the two nearest Nb neighbors with respect to the O vacancy by 6.5% of $a_0$. This is accompanied by much smaller, 0.9% outward displacement of K atoms and by 1.9% inward displacement of O atoms.[108,172–174] The two nearest Nb atoms give the largest ($\approx 80\%$) contribution to the lattice relaxation energy (3.7 eV) whereas O atoms give the most of the rest energy gain of 1 eV. The $F$ center in $KNbO_3$ produces a local energy level, which lies $\approx 0.6$ eV above the top of the valence band.[108,172–174] Its molecular orbital primarily contains contribution from the atomic orbitals of the two nearest Nb atoms.

Oxygen vacancies could be created in $PbZrO_3$ under neutron and ionizing irradiation.[175] Similarly to $PbTiO_3$, these defects make a major impact on the overall

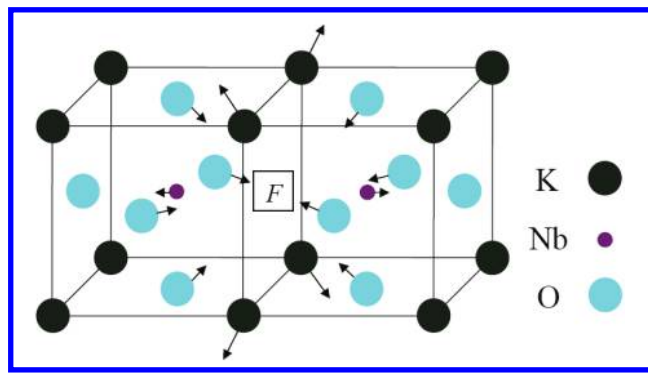


Fig. 6. Sketch of lattice relaxation around the $F$ center in $KNbO_3$.

]

performance of the ferroelectric devices based on $PbZrO_3$ or PZT.[176] However, no theoretical simulations on $PbZrO_3$ containing defects existed until recent DFT-LCAO calculations on the atomic and electronic structure of a $3 \times 3 \times 3$ times extended supercell of cubic $PbZrO_3$ containing $F$ centers.[177] The defect level of the $F$ center in cubic $PbZrO_3$ bulk lies quite deep, 1.72 eV below the CB bottom, in the calculated bandgap of 3.78 eV.[178] This defect level consists mainly of $6s$ and $6p$ orbitals of the nearest Pb atoms, with a small contribution of Zr $4d$ states.[177] An O vacancy in the bulk $PbZrO_3$ attracts $0.68e$, and the remaining electron density from the missing $O^{2-}$ is localized mostly on four nearest Pb atoms.[177] The two Zr atoms nearest to the defect in $PbZrO_3$ shift slightly outwards (by 0.48% of $a_0$) from the $F$ center, while the next four Pb atoms reveal substantial displacement (5.99% of $a_0$) toward the $F$ center. Deformation of the oxygen octahedra follows the displacement of Pb and Zr atoms. The $F$ center formation energy in the $PbZrO_3$ bulk is equal to 7.25 eV.[177]

The first *ab initio* calculations of oxygen vacancy on $ZrO_2$-terminated $PbZrO_3$ (001) surface were performed by Kotomin *et al.*[61] In this pilot study, the positions of all atoms surrounding the $F$ center on the $ZrO_2$ terminated surface were allowed to relax. As a result, the considerable outward relaxation is observed for the two Zr atoms nearest to the oxygen vacancy (8.46% of $a_0$), as well as for four nearest Pb atoms (11.97% of $a_0$).[61] The defect formation energy on the $ZrO_2$ terminated $PbZrO_3$ (001) surface containing the $F$ center (6–7 eV) depends on the SC size and is considerably smaller than that in the $PbZrO_3$ bulk (7.25 eV).[61] This is a driving force for the defect segregation to the $PbZrO_3$ surface. From the effective charge analysis, the conclusion could be drawn that only $0.3e$ is localized inside the surface oxygen vacancy, whereas the rest electron density of the missing $O^{2-}$ ions is delocalized over the nearest atoms.[61] Defect formation results in a slightly increased bandgap with respect to defectless surface structure. The surface $F$ center band for the $3 \times 3$ surface supercell in $PbZrO_3$ lies in the middle of the bandgap, namely 2.58 eV below the conduction band bottom.

The $F$ center energy level in the $SrTiO_3$ bulk bandgap approaches the CB bottom (being separated from it), moving from 0.69 eV for an 80-atom supercell (with the defect bandwidth of 0.15 eV), and finally reaching the optical ionization energy of 0.49 eV (with almost negligible bandwidth of 0.02–0.03 eV) for 270- and 320-atoms with the defect period close to four lattice constants.[180] DFT-PW calculations on 270- and 320-atom $SrTiO_3$ supercells give a reasonable estimate for the vacancy formation energy in the bulk, $E^{\text{form}}(F) = 7.1$ eV.[179] According to recent DFT-LCAO calculations on the cubic phase of $SrTiO_3$ perovskite by Carrasco *et al.*,[180] a Mulliken effective electronic charge of 1.1–1.3$e$ is localized inside the neutral O vacancy (depending on the supercell size) and 0.6–0.8$e$ are equally shared between the two nearest Ti ions. For a 320-atom $SrTiO_3$ bulk supercell, an expansion of the first coordination sphere (two Ti ions) (7.76% of $a_0$) and a compression of the second coordination sphere O atoms (7.79% of $a_0$) are comparable.

Table 14. Comparative analysis of main properties of bulk and surface $F$ centers in $SrTiO_3$, $PbZrO_3$, $PbTiO_3$ and $KNbO_3$ perovskites. Sign "+" corresponds to the expansion of atoms around the $F$ center.

| Property | $SrTiO_3$ | $PbZrO_3$ | $PbTiO_3$ | $KNbO_3$ |
|---|---|---|---|---|
| | | Bulk | | |
| Charge inside $V_O$ | 1.1–1.3[a] | 0.68[b] | 0.85[c] | 0.6[d] |
| $F$ distance to CB | 0.69–0.49[e] | 1.72[b] | 0.96[c] | 0.6 above the VB[d] |
| $F$ formation energy | 7.1[f] | 7.25[b] | 7.82[c] | — |
| B relaxation | +7.76[f] | +0.48[b] | — | +6.5[d] |
| O relaxation | −7.79[f] | — | — | −1.9[d] |
| A relaxation | +3.94[f] | −5.99[b] | — | +0.9[d] |
| | | $BO_2$-term (001) surf | | |
| Charge inside $V_O$ | — | 0.3[g] | — | — |
| $F$ distance to CB | 0.25[e] | 2.58[g] | — | — |
| $F$ formation energy | 6.22[e] | 6–7[g] | — | — |
| B relaxation | +14[e] | +8.46[g] | — | — |
| O relaxation | −8[e] | — | — | — |
| A relaxation | — | +11.97[g] | — | — |

[a]Reference 180. [b]Reference 177. [c]Reference 181. [d]Reference 108.
[e]Reference 178. [f]Reference 179. [g]Reference 61.

The outward relaxation of next neighbor Sr atoms (3.94% of $a_0$) are almost two times smaller.[179]

The formation energies for relaxed surface oxygen vacancy in $SrTiO_3$ are 6.22 eV for 120-atoms and 5.94 eV for 270-atom supercells.[178] The conclusion could be drawn that the defect formation energy on the $TiO_2$-terminated $SrTiO_3$ (001) surface is considerably smaller than in the $SrTiO_3$ bulk. The relaxation of the Ti and O atoms nearest to the surface $F$ center are (14% of $a_0$) (outwards) and (8% of $a_0$) (mainly inwards), respectively.[178] The defect ionization energy of the surface $F$ center on $TiO_2$-terminated $SrTiO_3$ (001) surface (0.25 eV) is about half that in the bulk. This is found for the 120-atom supercell, which is still far from convergence to the limit of a single defect. Here, the band dispersion is still not negligible (0.14 eV).[178]

The defect formation energy in $PbTiO_3$ bulk is equal to 7.82 eV,[181] and is approximately by 1 eV smaller than in the $SrTiO_3$ bulk. The $F$ center defect level position in $PbTiO_3$ bulk bandgap is located 0.96 eV below the CB bottom.[181] The Mulliken charge concentrated inside the O vacancy in $PbTiO_3$ bulk, according to *ab initio* calculations performed by Zhukovskii *et al.*[181] is 0.85$e$ (see Table 14).

### 3.5. *Computer modeling of hole and electron polarons in $ABO_3$ perovskites*

A transient optical absorption band at 1.2 eV in $KNbO_3$ has been associated,[182] in analogy with other perovskites, with a hole polaron (a hole bound, probably, to a

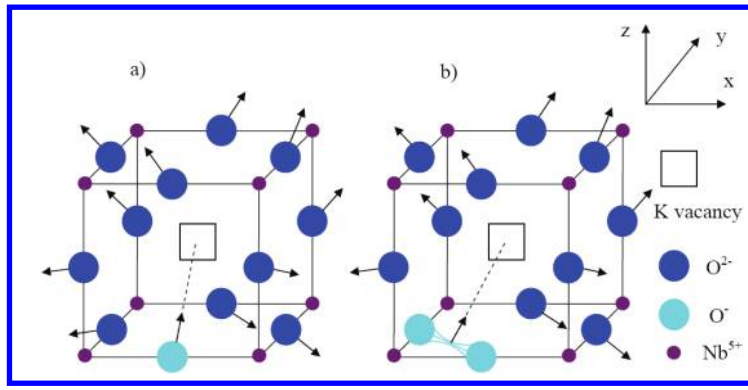


Fig. 7. Schematic view of the (a) one-site and (b) two-site hole polarons in $KNbO_3$.

K vacancy) (see Fig. 7). The electron spin resonance study of $KNbO_3$ doped with $Ti^{4+}$ gives a proof that holes could be trapped by such negatively charged defects.[183] The motivation for using the HF-based and DFT-based calculation methods[184,185] simultaneously is to combine strong sides of both in a single study. The DFT is expected to be able to provide a good description of the ground state. On the other hand, the HF formalism is straightforwardly suited for the evaluation of excited energies.[184]

The removal from the supercell of a K atom with its seven electrons contributing to the valence band (VB) produces slightly different effects on the electronic structure, as described within the DFT and the HF formalism.[185] In the INDO treatment, the one-electron optical gap is overestimated, as is typical for the HF calculations,[134] but the gap calculated as a difference of total energies in relaxed ground state and excited states ($\Delta$SCF gap) gives for the triplet state 2.9 eV, close to the experiment.[184] The INDO calculations in contrast to the LDA suggests, that the removal of an electron leaves an unpaired electron state split off at $\approx 1$ eV above the VB top.[184] The localized hole state is also present in the HF description but lies much lower than the corresponding state in the LDA, forming a 0.9 eV wide bandgap located $\approx 0.2$ eV below the conduction band bottom.[185]

In contrast to a generally observed large degree of covalency in $KNbO_3$ and contrary to a delocalized character of the $F$ center state,[108–110] the one-site polaron state remains well localized at the displaced O atom, with only a small contribution from atomic orbitals of other O ions but none from K or Nb ions. Despite that, there are some differences in the description of the electronic structure inside the DFT- and HF-based methods, the general trends in the total energy driving the structure optimization remain actually the same. In DFT and HF calculations,[184] both one-site and two-site configurations of the hole polaron are much more energetically favorable (see Table 15) than the fully symmetric relaxation of twelve O atoms around the K vacancy. This confirms what is already known about small-radius polarons in other ionic solids.[173,186–188]

Table 15. Absorption ($E_{abs}$) and lattice relaxation ($E_{rel}$, relative to the perfect crystal with a K vacancy) energies (eV), calculated by LMTO and INDO methods.

| Energy<br>Method | $E_{abs}$<br>Experiment | $E_{abs}$<br>INDO | $E_{rel}$<br>LMTO | $E_{rel}$<br>INDO |
|---|---|---|---|---|
| Uniform breathing | — | — | 0.01[b] | 0.08[b] |
| One-site polaron | 1.2[a] | 0.90[b] | 0.12[b] | 0.40[b] |
| Two-site polaron | — | 0.95[b] | 0.18[b] | 0.53[b] |

[a]Reference 182. [b]Reference 184.

Table 16. Optical absorption and lattice relaxation energies of electron polarons in $BaTiO_3$, $PbTiO_3$, $KNbO_3$ and $KTaO_3$ perovskites[192–195] as calculated by means of the INDO method. Sign "+" corresponds to expansion of atoms in the $x$–$y$ plane, and sign "−" corresponds to contraction of atoms in the $z$ plane in percents of the lattice constant $a_0$.

| Crystal | $E_{abs}$ | $\Delta$ in $x$–$y$ plane | $\Delta$ in $z$ plane | $E_{rel}$ |
|---|---|---|---|---|
| $BaTiO_3$ | 0.69[a] | 1.53[a] | −1.1[a] | 0.24[a] |
| $PbTiO_3$ | 0.73[b] | 1.46[b] | −1.04[b] | 0.22[b] |
| $KTaO_3$ | 0.75[c] | 1.70[c] | −1.2[c] | 0.27[c] |
| $KNbO_3$ | 0.78[d] | 1.40[d] | −1.0[d] | 0.21[d] |

[a]Reference 191. [b]Reference 192. [c]Reference 193. [d]Reference 194.

The existence of small radius polarons in ionic solids was predicted by Landau in 1933.[186] Strict experimental (ESR) proof of self-trapped *holes* was given for alkali halides by Känzig in 1957, a quarter of century later.[186] In 1994, the first ESR evidence appeared[189] for the electron self-trapping in $LiNbO_3$ perovskite crystals, accompanied by the IR absorption band around 1 eV. Finally, the $Nb^{4+}$ polaron absorption band around 0.72 eV has been observed recently in strontium barium niobate.[190]

The INDO simulations for electron polarons in $KNbO_3$, $KTaO_3$, $BaTiO_3$ and $PbTiO_3$ perovskite crystals were performed,[191–194] and the calculated energy gain due to electron self-trapping is 0.21, 0.27, 0.24 and 0.22 eV, respectively (see Table 16). The corresponding electron polaron absorption energies in $KNbO_3$, $KTaO_3$, $BaTiO_3$ and $PbTiO_3$ — 0.78, 0.75, 0.69 and 0.73 eV[191−194] agree well with the only experimental estimate of 0.6 eV for $BaTiO_3$.[195] For example, the electron polaron in $PbTiO_3$ were modeled using the $3 \times 3 \times 3$ extended cubic $PbTiO_3$ unit cell with the LUC containing 135 atoms. In order to find the energy minimum of the system, six nearest oxygen atoms in the octahedron around a central Ti atom were allowed to relax.[192] All other Ti and Pb atoms, as well as remaining O atoms, were kept fixed at their perfect lattice sites. According to INDO calculations,[192] the ground state is initially three-fold degenerate ($t_{2g}$). This degeneracy is lifted as a result of combined breathing mode and Jahn–Teller (JT) effects: Outward displacement of

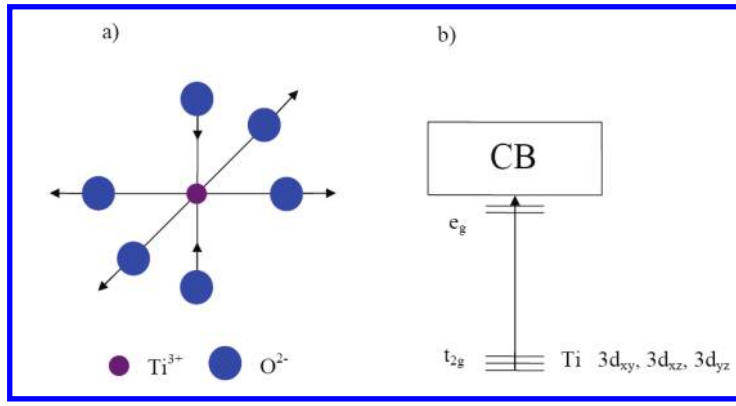


Fig. 8. (a) Sketch of the asymmetric O atom relaxations around an electron localized on the central Ti atom in the self-trapped electron in $PbTiO_3$. (b) Local energy states within the bandgap.

four nearest equatorial O atoms by 1.46% of $a_0$ and relaxation of the two oxygens inwards along the $z$ direction by 1.04% of $a_0$ (see Fig. 8). The total energy gain is 0.22 eV.[192] A similar JT electron polaron almost simultaneously was also observed experimentally in $BaTiO_3$.[196,197]

As a result, a considerable electron density in $PbTiO_3$ is localized on the central Ti atom[193] producing three narrowly spaced energy levels in the bandgap. They consist mainly of the $xy$, $xz$ and $yz$ Ti $3d$ atomic orbitals (split $t_{2g}$ energy level in an isolated ion); another two empty levels are located close to the conduction band bottom. The electron polaron absorption energy calculated by means of $\Delta$SCF method is 0.73 eV.[192] The absorption process corresponds to a charge transfer to the nearest Ti atom.

### 3.6. *Computer modeling of $KNb_xTa_{1-x}O_3$ solid solutions*

Figure 4 in Ref. 198 shows the total energy curve for a 135-atom $KTaO_3$ cluster doped with Nb modeling an isolated Nb impurity as a function of its [111] off-center displacement. The calculated displacement of 0.146 Å by Eglitis *et al.*[198–201] is very close to the experimental XAFS finding at 70 K.[95] The relevant energy gain is very small, only 0.0375 eV, which is a typical value for a Nb atom displacement as calculated earlier for different ferroelectric phases of $KNbO_3$.[134]

In order to calculate the Nb cluster (see Fig. 9) in the $KTaO_3$ matrix Eglitis *et al.*[198–201] have extended the primitive $KTaO_3$ unit cell by $4 \times 4 \times 4$, i.e., to 64 times its size, which is equivalent to carrying out the band structure calculations at 64 $k$-points in the Brillouin zone. In order to study the cooperative displacements (self-ordering) of Nb impurities in $KTaO_3$, seven Ta atoms were replaced by seven Nb atoms (see Fig. 10).

As a next step, in order to find the energy minimum of the seven atom Nb clusters in $KTaO_3$ matrix, six Nb atoms were allowed to relax symmetrically toward the central Nb atom. The positions of the K, Ta and O atoms were kept fixed. The

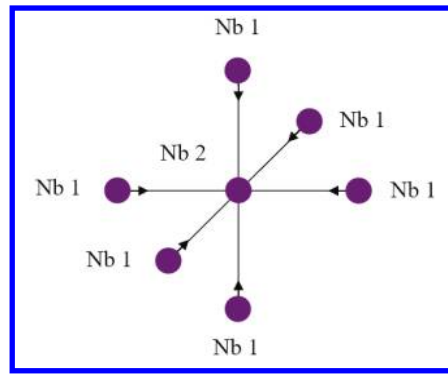


Fig. 9. Nb cluster containing seven Nb atoms inside $KTaO_3$ matrix.

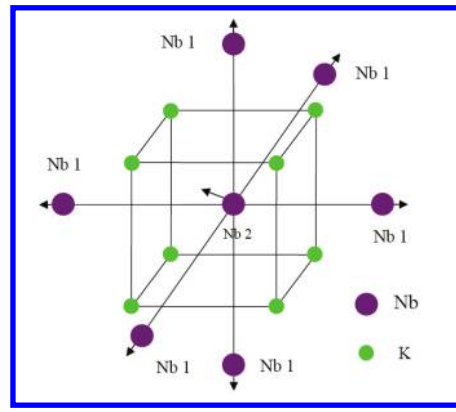


Fig. 10. Sketch of the symmetric repulsion of six Nb atoms outwards from the central Nb atom, which, as a consequence, is off-center them in both [100] and [111] directions.

results of numerical calculations show that six Nb atoms are displaced inwards toward the central Nb atom by 0.187 Å, lowering the total energy of the system by 0.088 eV. However, INDO calculations show that symmetric displacements of six Nb atoms outwards by 0.073 Å from the central Nb atom, lowering the total energy of the system by 0.03 eV, are also energetically favorable. In the case, when six Nb atoms are shifted outwards from the central Nb atom, the central Nb atom undergoes an off-center displacement from the on-site position in the [111] direction by 0.27 Å, and this is followed by an additional total energy gain of 0.09 eV — to give a total energy reduction of 0.12 eV.[99,102]

The central Nb atom reveals instability also in the [100] direction. The shift of the central Nb ion in the [100] direction by 0.192 Å additionally lowers the cluster energy by 0.056 eV, in the case when six Nb atoms are shifted outwards from the central Nb atom — to give a total energy reduction by 0.086 eV. Nevertheless, the total cluster structure induced energy lowering in the ground state, which corresponds to the situation in which six Nb atoms are symmetrically relaxed outwards

from the center of the Nb cluster, and the central Nb atom is displaced away from the center in the [111] direction (0.12 eV), is energetically more favorable.

According to the calculations performed by Eglitis *et al.*,[198,201] in the case when six Nb atoms are in the energy minimum state arising from a symmetric shift of six Nb atoms towards the central Nb atom (which could be treated as an excited state of the Nb cluster), the central Nb atom exhibits on-site properties.



## 4. Conclusions

In this paper, the present state-of-the-art in theoretical simulations of the $ABO_3$ perovskite surfaces and defects therein using (mostly) first principles modeling were illustrated. According to all calculations (see Table 4), on the AO-terminated (001) surface, all upper-layer A atoms relax inward for $SrTiO_3$, $BaTiO_3$, $PbTiO_3$, $CaTiO_3$ and $PbZrO_3$ perovskites by magnitude of at least 2% of the lattice constant $a_0$, while all second layer atoms relax outwards. For the $BO_2$-terminated $SrTiO_3$, $BaTiO_3$, $PbTiO_3$, $CaTiO_3$ and $PbZrO_3$ (001) surface, in most cases, the largest relaxations are on the second-layer metal atoms. For almost all $ABO_3$ perovskites, the (001) surface rumpling is much larger for the AO-terminated than for the $BO_2$-terminated (001) surface, but their surface energies are always quite similar.

In contrast, different terminations of the (011) $ABO_3$ surface lead to very different surface energies for the O-terminated, A-terminated, and BO-terminated (011) surface, respectively. A considerable increase in Ti–O or Zr–O, respectively, chemical bond covalency near the (011) surface as compared both to the bulk and to the (001) surface in $ABO_3$ perovskites were predicted.

For both B and $AO_3$-terminated $SrTiO_3$, $BaZrO_3$ and $SrZrO_3$ (111) surfaces the upper layer atoms, with the exception of the $BaO_3$ and $SrO_3$-terminated surface Ba and Sr atoms, respectively, relax inwards. For $SrTiO_3$, $BaZrO_3$ and $SrZrO_3$ (111) surfaces, the second layer Sr, Ba and Sr atoms exhibits the strongest relaxation between all atoms by 11.24, 9.73 and 11.92% of the lattice constant $a_0$, respectively. The most energetically favorable with the lowest surface energy, according to all performed calculations for all perovskites, always are the AO and $BO_2$-terminated $ABO_3$ perovskite (001) surfaces. The only exception is work by Zhang *et al.*,[59] where the O-terminated $CaTiO_3$ (011) surface is lower in energy than the $TiO_2$-terminated $CaTiO_3$ (001) surface. The A, BO and O-terminated $ABO_3$ perovskite (011) surfaces are always, according to all *ab initio* and shell model calculations, less energetically favorable than (001) surfaces. Finally, the $ABO_3$ perovskite (111) surfaces are always energetically most unfavorable and unstable surfaces according to all performed calculations.

Calculations performed in Ref. 106 demonstrate that Nb ions substituting for host Ti ions in $SrTiO_3$ are shallow donors. The symmetrical outward relaxation of six nearest O ions around the Nb impurity in $SrTiO_3$ crystal are very small.[106] In the Nb doped $SrTiO_3$ crystal negligible chemical bonding occurs between Nb and nearest O ions. It is interesting to note, that recent studies for the another impurity,

namely the Fe impurity in the $SrTiO_3$ crystal bulk[170] and on the surface[171] show that this is an acceptor. This demonstrates that the first-principles calculations are a reliable tool for studying the defects in perovskite materials.

A large amount of numerical calculations of mostly neutral bulk and surface oxygen vacancies performed so far for $SrTiO_3$, $PbTiO_3$, $PbZrO_3$ and $KNbO_3$ perovskites dealt with the local atomic structure and electronic density redistribution around defects in their regular lattice sites mainly after total or partial optimization of the defective structure geometry. All the calculation results for $F$ centers in $ABO_3$ perovskites are in sharp contrast with what is known about $F$ centers in ionic crystals (in particular, in MgO and alkali halides[202]) where the two electrons are well localized by the $V_0$ in the $F$ center ground state. Obviously, this discrepancy arises from a considerable degree of covalency of the chemical bonding in $ABO_3$ perovskites. Electron defects ($F$ centers) similar to what were observed in $ABO_3$ perovskites are known, for example, in partly covalent $SiO_2$ crystals (e.g., in the so-called $E_1'$ center an electron is also not localized inside $V_0$ but its wave function mainly overlaps with the $sp^3$ orbital centered on the neighboring Si atom[203]).

The quantitative models of hole polarons in $KNbO_3$ were analyzed.[184] The main conclusion is that both one-center and two-center hole polaron configurations in $KNbO_3$ are energetically favorable and close in energy. The calculated optical absorption energies and the spatial distribution of relevant electronic states could provide guidelines for more direct experimental identification of the defects in question. By means of the HF method calculated hole polaron absorption energy ($\approx 1$ eV) is close to the experimentally observed short-lived absorption band energy.[182]

The quantum chemical INDO calculations[191–194] gave additional evidence for the existence of electron polarons in $BaTiO_3$, $KNbO_3$, $KTaO_3$ and $PbTiO_3$ crystals. The theoretically calculated electron polaron absorption energy in $BaTiO_3$ (0.69 eV), $KNbO_3$ (0.78 eV), $KTaO_3$ (0.75 eV) and $PbTiO_3$ (0.73 eV) is close to the only experimental estimate of 0.6 eV for $BaTiO_3$.[195] The INDO calculated electron polaron absorption energies in $KNbO_3$, $KTaO_3$, $BaTiO_3$ and $PbTiO_3$ perovskites are smaller than the calculated and experimentally observed hole polaron absorption energies in $KNbO_3$. The electron polaron relaxation energies for $KNbO_3$, $BaTiO_3$, $PbTiO_3$ and $KTaO_3$ crystals are in the range from 0.21 eV till 0.27 eV.

The calculated magnitude of single Nb displacement (0.146 Å) in $KTaO_3$ matrix along the [111] direction is very close to the experimental XAFS finding of 0.145 Å observed at 70 K.[95] The interpretation of impurity-induced ferroelectric phase transition in terms of weak off-center impurities (like $Nb^{5+}$ impurities in incipient ferroelectric $KTaO_3$) had been suggested on the basis of the so-called self-ordered cluster model.[198–201] The main prediction of this model is that self-ordered clusters of the second component (Nb in $KTaO_3$) will form, which indeed were observed in calculations. Such self-ordered clusters of the second component in solid solutions based on ferroelectric perovskites have their own degrees of freedom. The percolation of the corresponding local order parameters as well as dynamical perco-

lation of the soft, low-frequency local vibrations can lead to a cooperative behavior which finally induces a ferroelectric phase transition.[198–201]

## Acknowledgments

This work was supported by the Latvian Council of Science Grant No. 374/2012 and ESF Grant No. 2013/0046/1DP/1.1.1.2.0/13/APIA/VIAA/021. The author is greatly indebted to D. Vanderbilt, K. M. Rabe, R. E. Cohen, M. R. Philpott, E. A. Kotomin, G. Borstel, J. Maier, R. Merkle, J. T. Devreese, N. E. Christensen, E. Heifets, A. V. Postnikov, D. Fuks, M. Rohlfing and S. Piskunov for fruitful discussions.

## References

1. J. F. Scott, *Ferroelectric Memories* (Springer, Berlin, 2000).
2. M. Dawber, K. M. Rabe and J. F. Scott, *Rev. Mod. Phys.* **77**, 1083 (2005).
3. R. E. Cohen, *Nat.* (*London*) **358**, 136 (1992).
4. C. Noguera, *Physics and Chemistry at Oxide Surfaces* (Cambridge University Press, New York, 1996).
5. M. E. Lines and A. M. Glass, *Principles and Applications of Ferroelectrics and Related Materials* (Clarendon, Oxford, 1977).
6. O. Auciello, J. F. Scott and R. Ramesh, *Phys. Today* **51**, 22 (1998).
7. N. Bickel, G. Schmidt, K. Heinz and K. Müller, *Phys. Rev. Lett.* **62**, 2009 (1989).
8. T. Hikita, T. Hanada, M. Kudo and M. Kawai, *Surf. Sci.* **287–288**, 377 (1993).
9. A. Ikeda, T. Nishimura, T. Morishita and Y. Kido, *Surf. Sci.* **433–435**, 520 (1999).
10. G. Charlton *et al.*, *Surf. Sci.* **457**, L376 (2000).
11. P. A. W. Van der Heide, Q. D. Jiang, Y. S. Kim and J. W. Rabalais, *Surf. Sci.* **473**, 59 (2001).
12. W. Maus-Friedrichs *et al.*, *Surf. Sci.* **515**, 499 (2002).
13. J. A. Enterkin *et al.*, *Nat. Mater.* **9**, 245 (2010).
14. H. Bando, Y. Aiura, Y. Haruyama, T. Shimizu and Y. Nishihara, *J. Vac. Sci. Technol. B* **13**, 1150 (1995).
15. K. Szot and W. Speier, *Phys. Rev. B* **60**, 5909 (1999).
16. J. Brunen and J. Zegenhagen, *Surf. Sci.* **389**, 349 (1997).
17. Q. D. Jiang and J. Zegenhagen, *Surf. Sci.* **425**, 343 (1999).
18. J. Zegenhagen, T. Haage and Q. D. Jiang, *Appl. Phys. A* **67**, 711 (1998).
19. R. Souda, *Phys. Rev. B* **60**, 6068 (1999).
20. Y. Adachi, S. Kohiki, K. Wagatsuma and M. Oku, *J. Appl. Phys.* **84**, 2123 (1998).
21. H. Tanaka and T. Kawai, *Surf. Sci.* **365**, 437 (1996).
22. J. Chang, Y. S. Park and S. K. Kim, *Appl. Phys. Lett.* **92**, 152910 (2008).
23. S. Kimura, J. Yamauchi, M. Tsukada and S. Watanabe, *Phys. Rev. B* **51**, 11049 (1995).
24. Z. Q. Li, J. L. Zhu, C. Q. Wu, Z. Tang and Y. Kawazoe, *Phys. Rev. B* **58**, 8075 (1998).
25. R. I. Eglitis and D. Vanderbilt, *Phys. Rev. B* **77**, 195408 (2008).
26. R. Herger *et al.*, *Phys. Rev. Lett.* **98**, 076102 (2007).
27. N. Erdman *et al.*, *Nat.* (*London*) **419**, 55 (2002).
28. T. Kubo and H. Nozoye, *Surf. Sci.* **542**, 177 (2003).
29. E. Heifets *et al.*, *Phys. Rev. B* **64**, 235417 (2001).

30. E. Heifets *et al.*, *Surf. Sci.* **513**, 211 (2002).
31. K. Johnston *et al.*, *Phys. Rev. B* **70**, 085415 (2004).
32. R. I. Eglitis *et al.*, *Ceram. Int.* **30**, 1989 (2004).
33. R. I. Eglitis *et al.*, *J. Electroceram.* **16**, 289 (2006).
34. S. Piskunov *et al.*, *Surf. Sci.* **575**, 75 (2005).
35. G. Borstel *et al.*, *Phys. Stat. Sol. B* **236**, 253 (2003).
36. R. Herger *et al.*, *Phys. Rev. B* **76**, 195435 (2007).
37. G. Borstel *et al.*, *J. Cryst. Growth* **237**, 687 (2002).
38. C. H. Lanier *et al.*, *Phys. Rev. B* **76**, 045421 (2007).
39. E. A. Kotomin, R. I. Eglitis, J. Maier and E. Heifets, *Thin Solid Films* **400**, 76 (2001).
40. Y. Li *et al.*, *Phys. Rev. B* **73**, 184112 (2006).
41. C. Cheng, K. Kunc and M. H. Lee, *Phys. Rev. B* **62**, 10409 (2000).
42. J. Padilla and D. Vanderbilt, *Surf. Sci.* **418**, 64 (1998).
43. B. Meyer, J. Padilla and D. Vanderbilt, *Faraday Discuss.* **114**, 395 (1999).
44. E. Heifets, E. A. Kotomin and J. Maier, *Surf. Sci.* **462**, 19 (2000).
45. V. Ravikumar, D. Wolf and V. P. Dravid, *Phys. Rev. Lett.* **74**, 960 (1995).
46. J. Padilla and D. Vanderbilt, *Phys. Rev. B* **56**, 1625 (1997).
47. R. I. Eglitis and D. Vanderbilt, *Phys. Rev. B* **76**, 155439 (2007).
48. F. Cora and C. R. A. Catlow, *Faraday Discuss.* **114**, 421 (1999).
49. L. Fu, E. Yaschenko, L. Resca and R. Resta, *Phys. Rev. B* **60**, 2697 (1999).
50. B. Meyer and D. Vanderbilt, *Phys. Rev. B* **63**, 205426 (2001).
51. C. Bungaro and K. M. Rabe, *Phys. Rev. B* **71**, 035420 (2005).
52. M. Krcmar and C. L. Fu, *Phys. Rev. B* **68**, 115404 (2003).
53. Y. Umeno, T. Shimada, T. Kitamura and C. Elsasser, *Phys. Rev. B* **74**, 174111 (2006).
54. R. I. Eglitis, *Integr. Ferroelectr.* **108**, 11 (2009).
55. B. K. Lai *et al.*, *Phys. Rev. B* **75**, 085412 (2007).
56. E. Heifets *et al.*, *J. Phys.: Condens. Matter* **10**, L347 (1998).
57. R. I. Eglitis and D. Vanderbilt, *Phys. Rev. B* **78**, 155420 (2008).
58. Y. X. Wang, M. Arai, T. Sasaki and C. L. Wang, *Phys. Rev. B* **73**, 035411 (2006).
59. J. M. Zhang, J. Cui, K. W. Xu, V. Ji and Z. Y. Man, *Phys. Rev. B* **76**, 115426 (2007).
60. A. Munkholm *et al.*, *Phys. Rev. Lett.* **88**, 016101 (2002).
61. E. A. Kotomin *et al.*, *Phys. Chem. Chem. Phys.* **10**, 4258 (2008).
62. R. I. Eglitis, *Integr. Ferroelectr.* **123**, 26 (2011).
63. Y. X. Wang *et al.*, *Surf. Sci.* **585**, 75 (2005).
64. R. I. Eglitis, *J. Phys.: Condens. Matter* **19**, 356004 (2007).
65. Y. X. Wang and M. Arai, *Surf. Sci.* **601**, 4092 (2007).
66. G. Pilania *et al.*, *J. Mater. Sci.* **44**, 5249 (2009).
67. R. A. Evarestov, A. V. Bandura and V. E. Alexandrov, *Phys. Stat. Sol. B* **243**, 2756 (2006).
68. R. I. Eglitis and M. Rohlfing, *J. Phys.: Condens. Matter* **22**, 415901 (2010).
69. A. Hofer *et al.*, *Phys. Rev. Lett.* **108**, 087602 (2012).
70. M. Stengal, *Phys. Rev. B* **84**, 205432 (2011).
71. R. A. Evarestov, A. V. Bandura and V. E. Alexandrov, *Surf. Sci.* **601**, 1844 (2007).
72. D. Li *et al.*, *Nat. Mater.* **7**, 473 (2008).
73. A. M. Kolpak *et al.*, *Phys. Rev. Lett.* **101**, 036102 (2008).
74. M. G. Brik, C. G. Ma and V. Krasnenko, *Surf. Sci.* **608**, 146 (2013).

75. J. A. Enterkin, A. E. Becerra-Toledo, K. R. Poeppelmeier and L. D. Marks, *Surf. Sci.* **606**, 344 (2012).
76. M. S. J. Marshall *et al.*, *Phys. Rev. B* **86**, 125416 (2012).
77. J. Ho, E. Heifets and B. Merinov, *Surf. Sci.* **601**, 490 (2007).
78. X. Wang, S. Tomado, T. Shimada and T. Kitamura, *Physica B* **410**, 22 (2013).
79. R. A. Evarestov, A. V. Bandura and D. D. Kuruch, *J. Comput. Chem.* **34**, 175 (2013).
80. J. He, G. B. Stephenson and S. M. Nakhmanson, *J. Appl. Phys.* **112**, 054112 (2012).
81. X. Wang, S. Tomoda, T. Shimada and T. Kitamura, *J. Phys.: Condens. Matter* **24**, 045903 (2012).
82. J. Wang, G. Tang and X. S. Wu, *Phys. Stat. Sol. B* **249**, 796 (2012).
83. F. Bottin, F. Finocchi and C. Noguera, *Phys. Rev. B* **68**, 035418 (2003).
84. E. Heifets *et al.*, *Phys. Rev. B* **69**, 035408 (2004).
85. E. Heifets, J. Ho and B. Merinov, *Phys. Rev. B* **75**, 155431 (2007).
86. A. Pojani, F. Finocchi and C. Noguera, *Surf. Sci.* **442**, 179 (1999).
87. W. Liu, C. Wang, J. Cui and Z. Y. Man, *Solid State Commun.* **149**, 1871 (2009).
88. R. I. Eglitis, *Ferroelectrics* **424**, 1 (2011).
89. R. I. Eglitis and M. Rohlfing, to appear in *Phys. Stat. Sol. B*, doi:10.1002/pssb.201248072.
90. R. I. Eglitis, *ab initio* calculations of $SrTiO_3$ (111) surfaces, *Proc. NATO ARW "Nanodevices and Nanomaterials for Ecological Security"*, eds. Y. N. Shunin and A. E. Kiv (Springer, Dordrecht, 2012), p. 125.
91. R. I. Eglitis, *Phase Trans.* **86**, 1115 (2013).
92. R. I. Eglitis, *Solid State Ion.* **230**, 43 (2013).
93. R. I. Eglitis, *Ferroelectrics* **436**, 5 (2012).
94. P. Günter and J. P. Huignard, *Photorefractive Materials and Their Applications*, Vols. 61–62 (Springer, Berlin, 1988).
95. O. Hanske-Petitpierre *et al.*, *Phys. Rev. B* **44**, 6700 (1991).
96. R. Niemann *et al.*, *J. Phys.: Condens. Matter* **8**, 5837 (1996).
97. P. Blennow *et al.*, *Solid State Ion.* **179**, 2047 (2008).
98. R. I. Eglitis and G. Borstel, *Phys. Stat. Sol. A* **202**, R13 (2005).
99. K. Szot *et al.*, *Nat. Mater.* **5**, 312 (2006).
100. I. Szafraniak *et al.*, *Appl. Phys. Lett.* **83**, 2211 (2003).
101. C. Binnig *et al.*, *Phys. Rev. Lett.* **45**, 352 (1980).
102. M. Takizawa *et al.*, *Phys. Rev. B* **79**, 113103 (2009).
103. R. Astala and P. D. Bristowe, *J. Phys.: Condens. Matter* **14**, L149 (2002).
104. A. S. Hamid, *Appl. Phys. A* **97**, 829 (2009).
105. X. G. Guo *et al.*, *Phys. Lett. A* **317**, 501 (2003).
106. R. I. Eglitis and E. A. Kotomin, *Physica B* **405**, 3164 (2010).
107. Y. Chen and M. M. Abraham, *J. Phys. Chem. Sol.* **51**, 747 (1990).
108. R. I. Eglitis *et al.*, *Phys. Rev. B* **56**, 8599 (1997).
109. H. Donnerberg and A. Birkholz, *J. Phys.: Condens. Matter* **12**, 8239 (2000).
110. E. A. Kotomin, R. I. Eglitis and A. I. Popov, *J. Phys.: Condens. Matter* **9**, L315 (1997).
111. V. R. Saunders *et al.*, *CRYSTAL2003 Users Manual* (University of Torino, Torino, 2003).
112. R. E. Cohen, *J. Phys. Chem. Solids* **57**, 1393 (1996).
113. R. E. Cohen, *Ferroelectrics* **194**, 323 (1997).
114. S. Piskunov *et al.*, *Comput. Mater. Sci.* **29**, 165 (2004).
115. R. Jia *et al.*, *Comput. Mater. Sci.* **73**, 9 (2013).

116. L. Yue *et al.*, *J. Phys. Chem. A* **114**, 8444 (2010).
117. H. Shi, R. Jia and R. I. Eglitis, *Phys. Rev. B* **81**, 195101 (2010).
118. H. Shi, R. I. Eglitis and G. Borstel, *J. Phys.: Condens. Matter* **19**, 056007 (2007).
119. H. Shi, R. I. Eglitis and G. Borstel, *J. Phys.: Condens. Matter* **18**, 8367 (2006).
120. R. I. Eglitis, H. Shi and G. Borstel, *Surf. Rev. Lett.* **13**, 149 (2006).
121. H. Shi, R. Jia and R. I. Eglitis, *Solid State Ion.* **187**, 1 (2011).
122. H. Shi, L. Chang, R. Jia and R. I. Eglitis, *J. Phys. Chem. C* **116**, 6392 (2012).
123. H. Shi, L. Chang, R. Jia and R. I. Eglitis, *J. Phys. Chem. C* **116**, 4832 (2012).
124. H. Shi, R. I. Eglitis and G. Borstel, *Comput. Mater. Sci.* **39**, 430 (2007).
125. A. D. Becke, *J. Chem. Phys.* **98**, 5648 (1993).
126. J. P. Perdew and Y. Wang, *Phys. Rev. B* **33**, 8800 (1986).
127. J. P. Perdew and Y. Wang, *Phys. Rev. B* **40**, 3399 (1989).
128. J. P. Perdew and Y. Wang, *Phys. Rev. B* **45**, 13244 (1992).
129. H. J. Monkhorst and J. D. Pack, *Phys. Rev. B* **13**, 5188 (1976).
130. C. Pisani (ed.), *Quantum-Mechanical Ab initio Calculations of the Properties of Crystalline Materials, Lecture Notes in Chemistry* Vol. 67 (Springer, Berlin, 1996).
131. A. Pojani, F. Finocchi and C. Noguera, *Appl. Surf. Sci.* **142**, 177 (1999).
132. A. Shluger, *Theoret. Chim. Acta* **66**, 355 (1985).
133. E. Stefanovich, E. Shidlovskaya, A. Shluger and M. Zakharov, *Phys. Stat. Sol. B* **160**, 529 (1990).
134. R. I. Eglitis, A. V. Postnikov and G. Borstel, *Phys. Rev. B* **54**, 2421 (1996).
135. M. Causa and A. Zupan, *Chem. Phys. Lett.* **220**, 145 (1994).
136. K. H. Hellwege and A. M. Hellwege (eds.), *Ferroelectrics and Related Substances*, Landolt-Bornstein, New Series Vol. 3 (Springer-Verlag, Berlin, 1969).
137. R. O. Bell and G. Rupprecht, *Phys. Rev.* **129**, 90 (1963).
138. G. J. Fischer, Z. Wang and S. Karato, *Phys. Chem. Miner.* **20**, 97 (1993).
139. B. G. Shirane and R. Repinsky, *Acta Cryst.* **9**, 131 (1956).
140. Z. Li, M. Grimsditch, C. M. Foster and S. K. Chan, *J. Phys. Chem. Solids* **57**, 1433 (1996).
141. B. J. Kennedy, C. J. Howard and B. C. Chakoumakos, *J. Phys.: Condens. Matter* **11**, 1479 (1999).
142. E. Cockayne and B. P. Burton, *Phys. Rev. B* **62**, 3735 (2000).
143. J. W. Bennett, I. Grinberg and A. M. Rappe, *Phys. Rev. B* **73**, 180102R (2006).
144. R. D. King-Smith and D. Vanderbilt, *Phys. Rev. B* **49**, 5828 (1994).
145. M. E. Björketun, P. G. Sundell and G. Wähnström, *Phys. Rev. B* **76**, 054307 (2007).
146. S. Piskunov *et al.*, *Comput. Mater. Sci.* **41**, 195 (2007).
147. S. S. N. Bharadwaja and S. B. Krupanidhi, *J. Appl. Phys.* **89**, 4541 (2001).
148. P. Ghosez, E. Cockayne, U. V. Wagmare and K. M. Rabe, *Phys. Rev. B* **60**, 836 (1999).
149. A. J. Smith and A. J. Welch, *Acta Crystallogr.* **13**, 653 (1960).
150. Z. Feng, H. Hu, S. Cui and C. Bai, *Solid State Commun.* **148**, 472 (2008).
151. R. Vali, *J. Phys. Chem. Solids* **69**, 876 (2008).
152. C. R. A. Catlow and A. M. Stoneham, *J. Phys. C* **16**, 4321 (1983).
153. R. C. Bochiccio and H. F. Reale, *J. Phys. B* **26**, 4871 (1993).
154. J. Muscat, A. Wander and N. M. Harrison, *Chem. Phys. Lett.* **342**, 397 (2001).
155. K. van Benthem, C. Elsasser and R. H. French, *J. Appl. Phys.* **90**, 6156 (2001).
156. S. H. Wemple, *Phys. Rev. B* **2**, 2679 (1970).
157. C. H. Peng, J. F. Chang and S. Desu, *Mater. Res. Soc. Symp. Proc.* **243**, 21 (1992).
158. Y. X. Wang, M. Arai and T. Sasaki, *Appl. Phys. Lett.* **88**, 091909 (2006).
159. O. Fursenko *et al.*, *Thin Solid Films* **520**, 4532 (2012).

160. Y. S. Lee *et al.*, *Phys. Rev. B* **67**, 113101 (2003).
161. M. Catti *et al.*, *J. Phys.: Condens. Matter* **3**, 4151 (1991).
162. M. Verstraete and X. Gonze, *Phys. Rev. B* **68**, 195123 (2003).
163. Y. X. Wang, *Phys. Status Solidi B* **244**, 602 (2007).
164. S. Tinte and M. D. Stachiotti, *AIP Conf. Proc.* **535**, 273 (2000).
165. J. M. Zhang, Q. Pang, K. W. Xu and V. Ji, *Comput. Mater. Sci.* **44**, 1360 (2009).
166. A. F. Fix *et al.*, *Phys. Scr.* **86**, 035304 (2012).
167. A. F. Vassilyeva, *Physica B* **405**, 2125 (2010).
168. H. Shi, L. Chang, R. Jia and R. I. Eglitis, *Comput. Mater. Sci.* **79**, 527 (2013).
169. A. S. Hamid, *Appl. Phys. A* **97**, 829 (2009).
170. R. A. Evarestov, S. Piskunov, E. A. Kotomin and G. Borstel, *Phys. Rev. B* **67**, 064101 (2003).
171. V. Alexandrov, R. A. Evarestov, E. A. Kotomin and J. Maier, *J. Phys. Conf. Ser.* **117**, 012001 (2008).
172. R. I. Eglitis, E. A. Kotomin and G. Borstel, *Comput. Mater. Sci.* **30**, 376 (2004).
173. E. A. Kotomin, R. I. Eglitis and G. Borstel, *Comput. Mater. Sci.* **17**, 290 (2000).
174. E. A. Kotomin *et al.*, *Comput. Mater. Sci.* **10**, 339 (1998).
175. R. Bittner *et al.*, *J. Appl. Phys.* **96**, 3239 (2004).
176. C. H. Ahn *et al.*, *Appl. Phys. Lett.* **70**, 206 (1997).
177. S. Piskunov *et al.*, *Comput. Mater. Sci.* **41**, 195 (2007).
178. J. Carrasco *et al.*, *Phys. Rev. B* **73**, 064106 (2006).
179. R. A. Evarestov, E. A. Kotomin and Y. F. Zhukovskii, *Int. J. Quantum Chem.* **106**, 2173 (2006).
180. J. Carrasco *et al.*, *Phys. Stat. Sol. C* **2**, 153 (2005).
181. Y. F. Zhukovskii, E. A. Kotomin, S. Piskunov and D. E. Ellis, *Solid State Commun.* **149**, 1359 (2009).
182. L. Grigorjeva, D. Millers, E. A. Kotomin and E. S. Polzik, *Solid State Commun.* **104**, 327 (1997).
183. E. Possenriede, B. Hellerman and O. F. Schirmer, *Solid State Commun.* **65**, 31 (1988).
184. E. A. Kotomin *et al.*, *Phys. Rev. B* **60**, 1 (1999).
185. R. I. Eglitis, E. A. Kotomin and G. Borstel, *Phys. Stat. Sol. B* **208**, 15 (1998).
186. A. L. Shluger and A. M. Stoneham, *J. Phys.: Condens. Matter* **5**, 3049 (1993).
187. J. T. Devreese *et al.*, *Phys. Rev. B* **63**, 184304 (2001).
188. G. Borstel, R. I. Eglitis, E. A. Kotomin and E. Heifets, *J. Cryst. Growth* **237–239**, 687 (2002).
189. B. Faust, H. Müller and O. F. Schirmer, *Ferroelectrics* **153**, 297 (1994).
190. M. Gao, S. Kapphan, R. Pankrath and J. Zhao, *Phys. Stat. Sol. B* **217**, 999 (2000).
191. R. I. Eglitis, E. A. Kotomin and G. Borstel, *J. Phys.: Condens. Matter* **14**, 3735 (2002).
192. R. I. Eglitis *et al.*, *J. Phys.: Condens. Matter* **14**, L647 (2002).
193. R. I. Eglitis *et al.*, *Comput. Mater. Sci.* **27**, 81 (2003).
194. E. A. Kotomin, R. I. Eglitis and G. Borstel, *J. Phys.: Condens. Matter* **12**, L557 (2000).
195. H. J. Reyher, Private Communication (2001).
196. S. Köhne *et al.*, *J. Supercond.* **12**, 193 (1999).
197. S. Lenjer, O. F. Schirmer, H. Hesse and T. Kool, *Phys. Rev. B* **66**, 165106 (2002).
198. V. S. Vikhnin, R. I. Eglitis, P. A. Markovin and G. Borstel, *Phys. Stat. Sol. B* **212**, 53 (1999).
199. R. I. Eglitis, E. A. Kotomin and G. Borstel, *J. Phys.: Condens. Matter* **12**, L431 (2000).

200. R. I. Eglitis *et al.*, *Mater. Sci. Semicond. Process.* **5**, 153 (2003).
201. R. I. Eglitis, E. A. Kotomin, G. Borstel and S. Dorfman, *J. Phys.: Condens. Matter* **10**, 6271 (1998).
202. J. H. Crawford, *Nucl. Instrum. Methods Phys. Res. B* **1**, 159 (1984).
203. K. L. Yip and W. B. Fowler, *Phys. Rev. B* **11**, 2327 (1975).

**This article has been cited by:**


1. Sergei Piskunov, Roberts I. Eglitis. 2015. First principles hybrid DFT calculations of BaTiO3/SrTiO3(001) interface. *Solid State Ionics* **274**, 29-33. [CrossRef]
2. Andrei V. Bandura, Dmitry D. Kuruch, Robert A. Evarestov. 2015. Quantum Chemical Study of Water Adsorption on the Surfaces of SrTiO 3 Nanotubes. *ChemPhysChem* n/a-n/a. [CrossRef]
3. A Bakulin, A Ponomarev, S Kulkova. 2015. Ab-initio Study of Cation-rich InP(001) and GaP(001) Surface Reconstructions and Iodine Adsorption. *IOP Conference Series: Materials Science and Engineering* **77**, 012004. [CrossRef]
4. David N. Mueller, Michael L. Machala, Hendrik Bluhm, William C. Chueh. 2015. Redox activity of surface oxygen anions in oxygen-deficient perovskite oxides during electrochemical reactions. *Nature Communications* **6**, 6097. [CrossRef]